Review

Contamination Level Monitoring Techniques for High-Voltage Insulators: A Review

Luqman Maraaba [1], Khaled Al-Soufi [2], Twaha Ssennoga [3,*], Azhar M. Memon [2], Muhammed Y. Worku [4] and Luai M. Alhems [2]

1   Department of Electrical Engineering, Arab American University, 13 Zababdeh, Jenin P.O. Box 240, Palestine
2   Applied Research Center for Metrology, Standards and Testing, Research Institute, King Fahd University of Petroleum and Minerals, Dhahran 31261, Saudi Arabia
3   Department of Architecture and Built Environment, Faculty of Engineering, University of Nottingham, Nottingham NG7 2RD, UK
4   Interdisciplinary Research Center for Renewable Energy and Power Systems (IRC-REPS), Research Institute, King Fahd University of Petroleum and Minerals, Dhahran 31261, Saudi Arabia
*   Correspondence: twaha.ssennoga1@nottingham.ac.uk or ssennogatwaha2007@gmail.com; Tel.: +44-7928531186

Abstract: Insulators are considered one of the most significant parts of power systems which can affect the overall performance of high-voltage (HV) transmission lines and substations. High-voltage (HV) insulators are critical for the successful operation of HV overhead transmission lines, and a failure in any insulator due to contamination can lead to flashover voltage, which will cause a power outage. However, the electrical performance of HV insulators is highly environment sensitive. The main cause of these flashovers in the industrial, agricultural, desert, and coastal areas, is the insulator contamination caused by unfavorable climatic conditions such as dew, fog, or rain. Therefore, the purpose of this work is to review the different methods adopted to identify the contamination level on high-voltage insulators. Several methods have been developed to observe and measure the contamination level on HV insulators, such as leakage current, partial disgorgement, and images with the help of different techniques. Various techniques have been discussed alongside their advantages and disadvantages on the basis of the published research work in the last decade. The major high-voltage insulator contamination level classification techniques discussed include machine learning, fuzzy logic, neuro–fuzzy interface, detrended fluctuation analysis (DFA), and other methods. The contamination level data will aid the scheduling of the extensive and costly substation insulator, and live line washing performed using high-pressured water. As a result, considerable benefits in terms of improved power system reliability and maintenance cost savings will be realized. This paper provides an overview of the different signal processing and machine-learning methods adopted to identify the contamination level on high-voltage insulators. Various methods are studied, and the advantages and disadvantages of each method are discussed. The comprehensive review of the islanding methods will provide power utilities and researchers with a reference and guideline to select the best method to be used for contamination level identification based on their effectiveness and economic feasibility.

Keywords: contamination level monitoring; high-voltage insulators; signal processing; machine learning

1. Introduction

Insulators are regarded as a highly significant power system component that can influence the general performance of the substations and transmission lines. For example, medical and steel mill electrical loads require an uninterruptible power supply. Therefore, any degradation in the insulator performance may result in a sizeable loss of service and revenue. There are two types of HV insulators based on the material used—ceramic and nonceramic insulators—and based on the place of installation in overhead transmission lines—pin, suspension, strain, and shackle insulators.

The electrical performance of HV insulators is highly environment sensitive. The withstand and flashover voltages of an insulator are reduced when it is polluted and wetted [1,2]. The conventional porcelain and glass insulators that have shown durability in field conditions are very heavy items that have quite a significant impact on the mechanical requirements of the HV transmission networks [3,4]. For the heavily contaminated conditions where much longer strings are required to be erected, the impact becomes quite limiting on the design parameters, and therefore, heavy reliance on expensive, tedious, and time-consuming maintenance programs becomes an essential part of the design consideration. Electric utility companies have the very challenging task of providing a reliable electric power supply to highly demanding consumers [5]. Moreover, the reliability requirements are becoming more stringent as the comfort of life becomes more and more power dependent. The electric companies, therefore, welcome any technological advancement in the insulator material which could facilitate their professional understanding with ease without compromising the reliability of the power system. Since the 1960s, composite insulators have been introduced as a potential replacement for conventional porcelain and glass insulators. These insulators offer several advantages in terms of being lightweight, easy to handle, resistant to vandalism, and relatively low cost [6–8]. Various materials such as ethylene propylene diene monomer (EPDM), room-temperature-vulcanized (RTV) silicon rubber, and heat transfer vinyl (HTV) silicone rubber were employed to manufacture the polymeric insulators [5,9–11].

The design and construction of overhead transmission lines have several technical, economic, and environmental constraints. In densely populated areas, for example, it is essential to decrease the width of the right-of-way and to consider the visual impact of the line [12]. In remote and less accessible areas, it is imperative to ensure that transmission lines are of high mechanical and electrical performance. The selection of insulators has a significant effect on overall line design. Porcelain and glass insulators have evolved over the years, and their design has been adapted to increasing transmission voltages. The composite long–rod insulators, because of their lightweight and high mechanical strength, are an attractive alternative to conventional glass and porcelain insulators for transmission lines [13]. The economic benefits of composite insulators also allow the possibility of building compact towers. Apart from these advantages, composite insulators can be expected to provide satisfactory insulating behavior under polluted conditions for a given creepage path, owing to their slender shape and resultant high form factor. Additionally, long creepage paths exist, as sheds of complex shapes can be easily fabricated. Additionally, losses due to leakage current are reduced compared with large-surface insulators. Composite insulators also offer low shock sensitivity with respect to mechanical shocks such as the impact of a rifle bullet. Because of their light weight, transportation and installation of emergency towers insulated with polymeric insulators can be implemented very efficiently in remote areas by utilizing helicopter services. However, an important problem with synthetic insulators is their sensitivity to atmospheric influences under electric stress. In contrast to ceramic materials, plastics may be damaged under combined electric and atmospheric stresses, leading to a reduction in their useful life [14].

The Kingdom of Saudi Arabia has undergone a rapid industrialization program in the last decade. During the 2008–2018 period, the total energy sales increased at a faster rate from 187 TWh to 299 TWh, representing an increase of 59.9%. To keep up with the increased energy needs, high-voltage (HV) overhead transmission lines were constructed in the Kingdom at a much faster pace. Insulators are one of the most important elements in the transmission system [15,16]. The Kingdom of Saudi Arabia's climatic conditions and geography are distinctive, with enormous deserts bordered mostly by the sea. Typical climatic conditions are characterized by extreme ambient temperatures with significant variations between day and night, extensive changes in relative humidity, strong winds carrying dust and sand particles, suspended dust particles, a few days with mist and fog, and mostly sunny days during the year. The consumers of electric power in the Kingdom are mainly clustered around the two coastal areas at the Red Sea and the Gulf and around

the capital city of Riyadh in the central region. The airborne contamination particles are also brought by the wind to the vicinity of an insulator string, where, under the influence of electrostatic, gravitational, and frictional forces, the particles are attached to the insulator surfaces. In the presence of moisture caused by light rain, high relative humidity, fog, etc., adhesive soluble particles form conducting layers on the insulator surface, permitting the leakage current. Because of the inherent nonhomogenous distribution of contaminants and moisture experienced by an energized insulator string, the degree of evaporation by Joule's heating varies, resulting in the formation of dry band(s). Across the dry band, a relatively high voltage builds up, which may reach a critical value, where air ionization sets in and bridges the gap. This process can be repeated until, under some unfavorable conditions, air ionization develops into a partial discharge propagating into a flashover [1,17,18].

According to the literature, many methods have been used in monitoring the contamination level of the insulators. Some of the methods are thermal imaging, ultraviolet imaging, digital imaging, ultrasonic signal, acoustic signals, leakage current, and partial discharge [19–25]. Numerous laboratories and utilities use the magnitude of the leakage current (LC) caused by contamination on the insulator surface as a gauge for contamination level, surface wear, or the general status of the insulator and its performance.

Observing and measuring the contamination levels in high-voltage insulators are very crucial because of the following reasons:

- To prevent disastrous flashovers and decreases compulsory outage period by providing correct and precise information about the pollution level ahead of time;
- To decrease maintenance costs and enable effective maintenance planning (specify the optimal time for washing);
- To improve the general dependability of the electrical system;
- To enable effective utilization of limited resources, such as workforce and time, by creating priorities for the upkeep of insulators.

2. The Insulator Contamination and Source of Contaminants

The source of contamination of insulators refers to the type of substance that causes the contamination of an insulator, such as cement, sand, dust, industrial pollution, and agricultural pollution. These contaminants can affect the insulator's performance [26,27]. Insulator pollution is usually gauged in terms of equivalent salt deposit density (ESDD) and expressed in mg of salt (NaCl) per sq cm. of the surface area of the insulator [28,29]. It has been observed that in some coastal areas, the insulator contamination level accumulates to the ESDD level greater than 0.1 mg/cm^2 in two months [30], warranting exclusive consideration to lessen their effect on the power system. The online contamination level monitoring data help with the scheduling of the extensive and costly substation insulator, and live line washing performed using high-pressured water. Therefore, positive results are obtained in terms of improved power system reliability and maintenance cost savings.

Tables 1 and 2 show the IEC-60815, CIGRE, and IEEE classification of contamination severity [31–33].

Table 1. The IEC 60815 standard for contamination level classification [31–33].

IEC 60815 Standards		
Leakage Distance (kV/l mm)	ESDD (mg/cm^2)	Site Severity
2.11	>0.40	Very Heavy
1.70	0.15–0.40	Heavy
1.37	0.04–0.15	Medium
1.09	0.01–0.04	Light
0.87	<0.01	Very Light

Table 2. The CIGRE and IEEE standards for contamination level classification [31–33].

ESDD, mg/cm^2		Site Severity
IEEE	**CIGRE**	
-	>0.48	Exceptional
-	0.24–0.48	Very heavy
>0.10	0.12–0.24	Heavy
0.06–0.10	0.06–0.12	Average/Moderate
0.03–0.06	0.03–0.06	Light
0–0.03	0.015–0.03	Very light
-	0.0075–0.015	None

3. Industry Experience in Improving Insulator Performance

The disturbance resulting from insulator arcing caused by pollution flashover (FOV) is amongst the issues faced by high-voltage grid engineers. The insulator flashover is a serious problem whose occurrence is determined by various factors, insulator design, operating conditions, nature of the region, and weather conditions [34,35]. One of the most common methods applied as a solution for this problem at the design level utilities the leakage distance extension. While addressing the problem of pollution, the nature of the pollution in the high-voltage line needs to be identified first. Because of the severe pollution conditions, the outdoor insulation coordination necessitates a clear geographic mapping of the natural pollution deposit as well as comprehensive statistical studies [36]. The sampling methods, classification s as well as ranking charts are prepared to establish the severity of the environment. It is the role of maintenance crews and design engineers to find out how electric flashovers should be prevented. The performance of HV insulators can be improved by either improving insulator insulation or preventing conductive layer formation. Different ways, such as coating, creepage extenders, optimization of electric field distribution, and cleaning, have been used by power utilities to improve the insulators' performance [37].

3.1. Coating of Insulator

The hydrophobic material was added to the insulators' surface to improve the performance of the ceramic insulator. Among the popularly employed SiR in various applications and electrical systems are; room-temperature-vulcanized silicone rubber (RTV-SiR) and high-temperature-vulcanized silicone rubber (HTV-SiR). Out of all the silicone rubbers, HTV and RTV silicone are highly recommended because of their better characteristics compared with others in terms of compressive mechanical behavior, better curing, high tensile strength, actuation, easy processing, and better hydrophobicity. The RTV silicon rubber is frequently applied for ceramic insulator spraying and coating because it usually drys very fast. But for HTV, it is the manufacturing process for composite insulators under high temperature and high pressure as per standards [38]. Subsequently, the materials offer a hydrophobic surface that prevents the conducting layer formation. Consequently, the size of the leakage current flowing on the insulator surface is reduced, lowering the probability of a flashover [39]. Table 3 shows the leakage current magnitude on coated and noncoated insulators as a function of applied voltage. Results showed that the coated insulator has less leakage current compared with the noncoated insulator at the same voltage level [40].

The effect of using RTV silicon rubber coating of ceramic insulators on the leakage current magnitude was investigated in [40]. It was concluded that using grease silicon as a coating material is not economical as it has to be replaced in a short period of time, typically every six months, because of its limited lifespan. Thus, the advantage of using the RTV silicon rubber is that its lifetime is longer, exceeding five years. The selection of the optimum time for replacing the coating is still a topic for research [41]. Moreover, the application and removal of the coating due to excess lifespan are complicated [9].

Table 3. The magnitude of insulator leakage current.

Leakage Current (mA) RTV Coated	Leakage Current (mA) Noncoated	Voltage (kV)
0.811	-	45
0.705	-	40
0.580	Flashover	35
0.478	-	30
0.394	1.601	25
0.305	0.695	20
0.224	0.371	15
0.151	0.358	10
0.073	0.226	5

3.2. Optimization of Electric Field Distribution

A method for optimizing the distribution of electric field along composite insulators was proposed in [42], where the finite element method is used. A three-dimensional model for the computation of the electric field was derived, whereas the surface voltage distribution along the composite insulator was determined. It was concluded, from the results, that the electric field towards the end of the composite was significantly reduced because of the increase in the number of combined glass insulators.

Table 4 indicates the electric field strength reduction due to various glass insulator installations at a voltage level of 500 kV, in which n represents the number of units of insulators connected in series [41].

Table 4. Insulator's electric field strength reduction when different glass insulators are installed.

n	4	3	2	1	0
Voltage of 20% distance in high voltage end %	38.36	41.61	45.44	51.75	63.5
Maximum electric field Strength (kV/mm)	0.39	0.536	0.65	1.01	2.0
% Voltage of composite insulator	53.26	57.91	63.76	73.62	100

3.3. Creepage Extenders

The flashover voltage will be adjusted by changing the creepage distance of the insulator, thereby reducing the leakage current and improving the strike distance as well as the insulator shape. Depending on the insulator type, the creepage extender is manufactured with semirigid polymer or flexible polymeric skirts. The creepage extenders are expensive and only used when other techniques are not possible. Figure 1 indicates the results of the flashover test performed on 66 kV post insulators with different creepage distances and a constant contamination level determined by the IEC507 standard. It is indicated that the flashover voltages increase when the creepage distances increase [9,41].
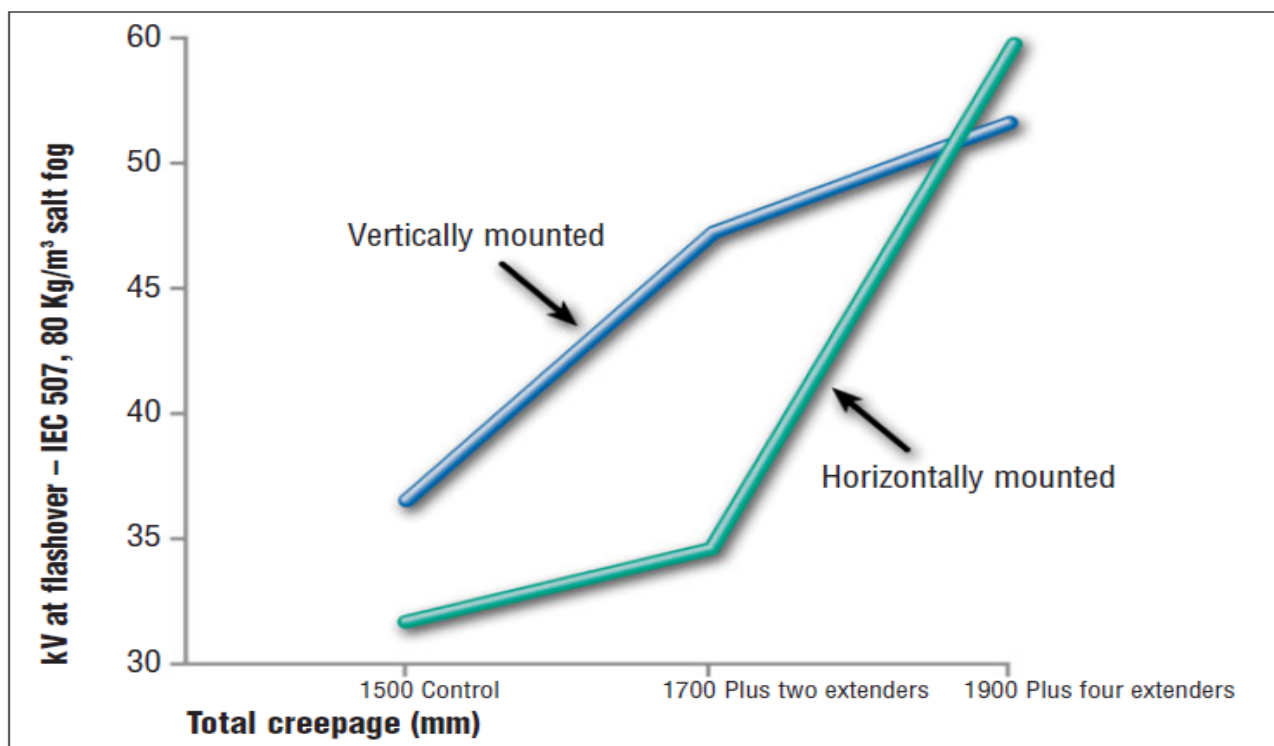
Figure 1. Flashover voltage against the number of extenders of a post insulator at 66 kV [9].

3.4. Washing of Insulator (Cleaning)

This technique allows insulator washing while the electrical lines are still energized, and it reduces line outages caused by switching the lines off for offline insulator washing. The live line insulator washing is conducted using high-resistivity pressurized water jets at a nozzle pressure of about 550pa [43]. Under special conditions that lead to sudden contaminant accumulation on the insulators, emergency washings are employed. The two most popular techniques are listed in Table 5 [44].

Table 5. The insulator washing methods.

	Cleaning Method	Deposit	Comments
Insulator washing	High-pressure washing	Deposits with poor adhesion	Time of washing Live washing? Work hours cost if power interruptions are required
Insulator cleaning	Dry cleaning	Cement fertilizers	Time of cleaning Dry material deposits Cost Glaze damage and insulator shattering

3.5. The Saudi Electricity Company (SEC) Experience

The Saudi Electricity Company (SEC) was established in January 2000 as the only electricity company in the Kingdom of Saudi Arabia. The power transmission system in this area operates at voltage levels of 69, 115, 230, and 380 kV and consists of long transmission lines, most of which were built close to the coast of the Arabian Gulf. Some of the industrial loads, especially in the Jubail industrial area, are process industries, which are critically sensitive to voltage fluctuations (dips) and power outages. This fact makes resistance to contamination the most important factor in selecting transmission lines and substation insulators. Strict insulator specification is imposed to maintain good reliability of the HV power transmission system. In the late 1970s and early 1980s, the electricity service provider in Saudi Arabia experienced a high rate of pollution flashovers. In addition, a lack

of experience in maintaining the insulators and a limited number of available washing rigs and personnel all contributed to reducing the power system reliability. The weather-related transmission line interruption rate at that time was as high as 12 interruptions per 100 km per year. In addition, major power system disturbances were experienced in 1985 because of the abovementioned reasons [45].

Eventually, SEC was required to manage the insulator contamination problem using cost-effective high-pressure live line washing. As mentioned earlier, this was realized by means of high-resistivity pressure jets with roughly 550 psi pressure at the outlet. The frequency of washing jobs is related to the line's criticality and the extent of insulator contamination [16,45]. Accordingly, wash zones have been classified, and the respective wash intervals in those zones vary from one month to twelve months as follows [45]:

- Zone 1—Washing every month: line insulators near major generating plants, such as Ghazlan Power Plant, and in close proximity to the Arabian Gulf;
- Zone 2—Washing every 2–3 months: line insulators near major generating plants, such as Berri Power Plant, but not too close to the Arabian Gulf;
- Zone 3—Washing every 6–12 months: line insulators at a distance of 20–50 km from the Arabian Gulf;
- Zone 4—No washing: Lines located more than 50 km from the Arabian Gulf.

In extraordinary and special situations, emergency washings are needed as well. The occurrence of a "Shamal" (northwesterly wind) can, for instance, cause an abrupt contaminant accumulation on the insulators, which requires urgent washings. The annual power interruptions associated with pollution-related insulator flashovers had been reduced from about 1.22 interruptions per 100 km per year in 1979 to 0.53 interruptions per 100 km per year in 2001 [16,46] as a result of insulator washing and adopting improved insulator design. However, this performance improvement was achieved with a substantial increase in the maintenance cost. Implementation of live line and substation insulator washing, successive enhancements in the washing expertise, proper equipment upkeep, and lastly, optimized schedules of washing added considerably to the overall transmission system reliability. It has already been established that insulator washing is an extremely effective but very costly method; For SEC, the annual incurred cost is about SAR 15 million, which roughly equals USD 4 million. Note that this does not account for the substation insulator washing [47].

4. Contamination Indicators & Signal Processing Techniques

One of the critical aspects for reliable operations of high-voltage equipment is contamination monitoring and prediction and cleaning of the high-voltage insulators. Specifically, the prediction and monitoring capability allows the electric utilities to have an optimized schedule for washing live lines and substation insulators. This translates into significant cost savings while improving the electrical system's reliability by preventing disastrous flashover events. In what follows, various indicators used for insulator contamination assessment and the related signal-processing techniques are discussed using a comprehensive account of the relevant literature. Figure 2 shows the different contamination level monitoring methods.

4.1. Leakage Current

The magnitude of leakage current (LC) developed on the insulator surface due to contamination is used by various independent laboratories, universities, and power utilities as an indicator of surface degradation, insulation pollution severity, and insulator performance [3]. The "dry banding" and thermal effects of the leakage current on the contaminant result in the nonlinearity of voltage distribution. Subsequently, the entire insulator or only its portion is covered by the dry band, resulting in a flashover [48,49]. At less than 90% of relative humidity, the LC is observed to be an unsuitable method to determine the contamination level [50,51]. The aging cycles modeled for a 500 kV line with lower contamination levels have revealed substantial degradation of some insulators nearer

to the live end, although insignificant LCs were recorded [52,53]. Moreover, the existence of supplementary electromagnetic waves in the site greatly affects the LC measurements. Correspondingly, the reconstruction of an insulator and special arrangements have to be made to install the LC apparatus [54].
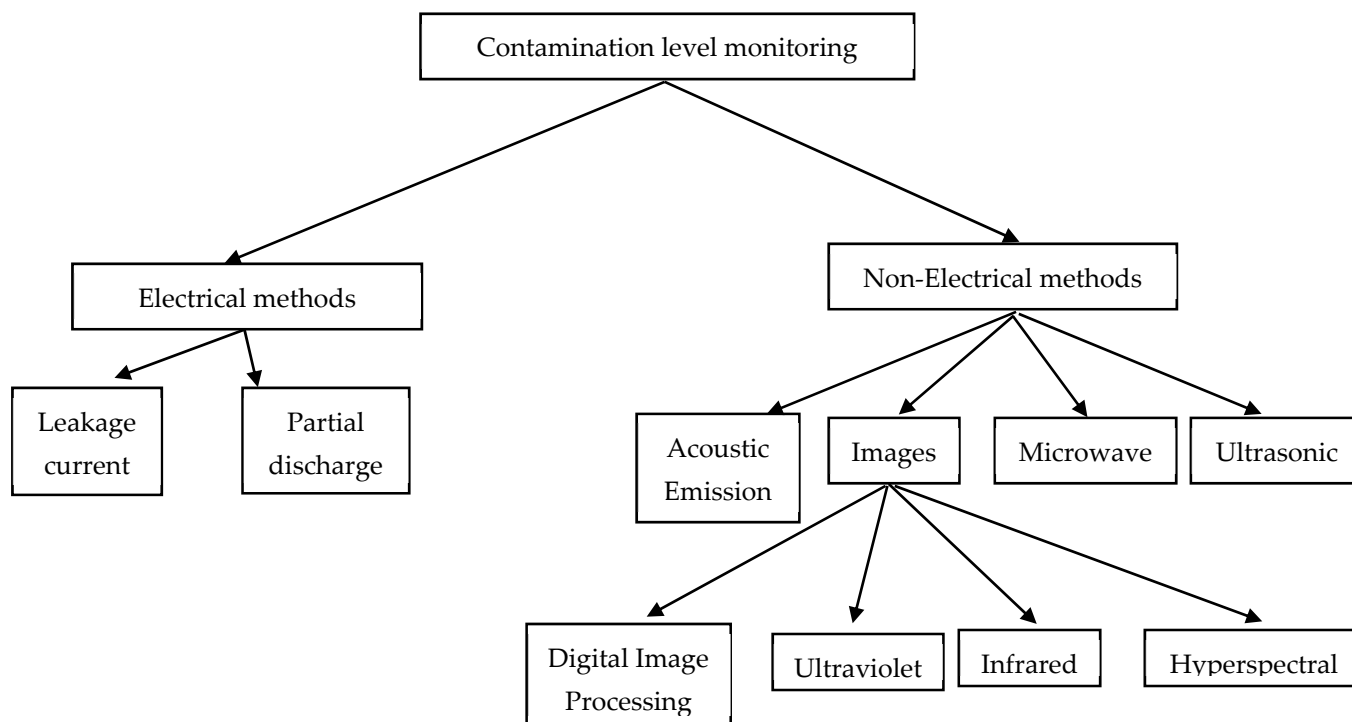
Figure 2. Different contamination level monitoring methods.

4.1.1. Fast Fourier Transform (FFT)

For FFT analysis of the leakage current, the odd harmonics of the FFT of LC are analyzed to categorize different contamination levels. Most of the works consider direct measurement of the LC; however, one study used a Rogowski coil [55] to indirectly measure the leakage current using an induced voltage in the coil. This technique was reported to be simple, cost effective, and did not require signal reconstruction before the computation of FFT. In [56], 12 insulators with four different equivalent salt deposit density (ESDD) values, 0.05 mg/cm^2, 0.1 mg/cm^2, 0.2 mg/cm^2, and 0.3 mg/cm^2, were tested under wet (relative humidity (RH) = 98%) and dry (RH = 50%) conditions. It was found that only qualitative categorization among ESDD levels was possible as light and heavy contamination, and the exact value of ESDD could not be obtained from LC. Other findings revealed that the total harmonic distortion (THD) could not be used in dry or wet conditions, and the ratios of fundamental to fifth and third harmonics were useful for dry and wet conditions, respectively. In [57], LC was studied as a function of humidity, applied voltage, and contamination defined in terms of ESDD. Humidity values used were 30, 60, 70, 80, and 90%, and ESDD was varied as very low, low, moderate, high, and very high. THD was also studied as a function of humidity at a constant level of contamination. It was found that the LC level was directly proportional to humidity, voltage, and contamination level, while the flashover voltage was inversely proportional to ESDD. For the noncontaminated insulator, it was observed that the third harmonic magnitude was less than that of the fifth and 7seventh harmonics, whereas, for the contaminated insulator, the opposite was true. Moreover, a higher THD for higher humidity levels was observed.

Results in [58] confirmed the results reported in [59] by comparing the performance between two types of contaminants, NaCl and CuSO4, for an 11 kV glass disc insulator contaminated at three different values. The main findings were that the probability of

flashover and THD was higher in the case of NaCl compared with CuSO4. Similar to the findings of [57], the magnitude of the third harmonic was less than that of the fifth harmonic at clean or low-contamination levels; however, for a highly contaminated insulator, the third harmonic component became critical to forecast the pollution level of the insulator. In terms of the growth of harmonics, it was observed that the growth of the third and fifth harmonics was uniform and rapid for NaCl but nonuniform for the third harmonic in the case of CuSO4. Based on these findings, it was concluded that the fifth to third harmonic component ratio was important for predicting the flashover condition. The main shortcoming was that only the flashover probability, but not the magnitude of LC, was compared for both contamination types.

In [55], both soluble and nonsoluble contaminations were considered by using NaCl for the former and fine-grinded charcoal for the latter to emulate the cases where insulators are operational near charcoal manufacturing factories and rice ash burning. The authors used Rogowski's coil to measure the LC. The induced voltage in the coil was analyzed by FFT on the basis of the idea that the distortion of voltage increases proportionally to the contamination levels due to significant dry band arcing, thus serving as an indicator of the contamination level. Similar to the previous works cited above, it was observed that an increase in the contamination level increased the third harmonic amplitude of the voltage signal compared with the fifth harmonic, making the ratio of these two harmonics critical for contamination monitoring. The same results were reported in [60].

In [61], a composite insulator FXBW-110/100 was studied under different contamination and hydrophobic levels. Pulse amplitude, energy ratio, and energy were extracted from LC and considered characteristic parameters for contamination and hydrophobic levels. In [62], it was reported that the even harmonics of the LC were lower in amplitude compared with the odd ones, where the third, fifth, and seventh harmonics were dominant.

4.1.2. Time Domain Analysis of LC

In [63,64], toughened glass and porcelain insulators for 35 kV transmission lines were tested in an artificial fog chamber with salt contamination. A total of 11 insulators were considered with five ESDD values (0.03, 0.05, 0.1, 0.2, and 0.3 mg/cm^2). A large number of tests were repeated to arrive at the LC boundary values in the time domain to categorize the contamination levels. It was found that the 50–150 mA range could be divided into the first stage, "Security Stage" < 50 mA, the second stage, "Forecast Stage" 50–150 mA, and the third stage, "Danger Stage" > 150 mA. LC waveforms were also observed at these stages, where sine or triangular shapes was observed at the Security Stage. At the Forecast Stage, a significant number of high-frequency spikes were seen, mainly in the wave crest high enough to make zero crossing, and at the Danger Stage, LC showed similar sinusoidal shapes as the first stage and the current increased. Similarly, in [65], it was found that close to the flashover stage, the LC waveform becomes a sine wave with an increased amplitude.

An investigation of the LC at different RH levels to categorize the contamination levels by current pulses was reported in [66]. Principal component analysis (PCA) was used to extract the pulse information, whereby it was shown that the principal components were highly correlated with the contamination levels. In [67], the relation between LC, ambient temperature, and humidity was investigated. A direct relationship between the current and humidity was observed, whereas a negative correlation was reported between the LC and temperature.

4.1.3. Wavelet Transform

In [68], the LC of 22 kV distribution insulators was collected during a six-month period at a sampling rate of 6.4 kHz. Discrete wavelet transform (DWT) was used to extract the current components related to the contamination levels, and the results showed high accuracy. DWT was also used in [69] to extract the contamination level index. As opposed to the spectral analysis, where low-frequency components are focused on the basis of the fact that they contain significant signal information compared with the higher harmonics, in this

paper, high-frequency components of the LC were proposed to assess the contamination levels. To mitigate the noise from the LC signal and compress it, the wavelet analysis method was used in [70]. Experiments showed a good correlation between the current and contamination levels. In [71], wavelet transform was used to analyze the LC collected from salt–fog tests along with the presence of nonsoluble contamination on ceramic and polymeric (SIR) insulators. The current signal was divided into the local arc and sinusoidal component; besides surface resistance and charge measurement, the LC surge counting, and peak recording were used to monitor the contamination levels. It was shown that the cumulative charge and the components were highly related to hydrophobicity and contamination level. In [72], the LC and its nonlinear characteristics were investigated to monitor the performance of suspension ceramic insulators (XWP2-70) in heavy salt–fog setting along with nonsoluble contamination. The spectral information of the flashover process was obtained using wavelet transform and visualized using a recurrent plot, which showed that the high-frequency components were highly correlated with the transition to flashover.

Wavelet fractal dimension, calculated as the sum of high-frequency values of the signal, was used in [73] for the analysis of the insulator state. The results showed that the fractal dimension effectively describes the arcs discharge in LC and is also a good eigenvalue for flashover discrimination and risk prediction.

4.1.4. S Transform

The main limitation of FFT is its applicability to only stationary signals where the spectral properties do not change over time. However, LC is known to be nonstationary, making FFT an inadequate methodology to effectively track the magnitude, frequency, or phase changes. On the other hand, wavelet transform depends on the selection of a suitable wavelet and gives sparse information with nonunique spectral regions. S transform overcomes these drawbacks and is suitable for transient analysis with the presence of noise.

In [74], tests were conducted on an 11 kV silicone rubber insulator for various pollution levels. S transform was successfully used to analyze LC to investigate the threshold at which the current transitions to severe arcing with increased contamination level. The effectiveness of the transform was reported, and the results showed that the surface condition of insulators could be easily identified.

Table 6 shows the comparison between the abovementioned signal processing techniques for leakage current in terms of accuracy. It can be observed that when mathematical morphological function and statistical operations are used in the preprocessing stage to test the porcelain insulator, the highest accuracy of 100% is obtained while the lowest accuracy (2%) is achieved when FFT signals are used to test the porcelain, glass, and polymer insulators.

Table 6. The comparison between different signal processing techniques for leakage current in terms of accuracy.

Reference	Insulator Type	Preprocessing Stage	Metrics	Accuracy
[75]	Porcelain	Time domain analysis and discrete wavelet transform	Out-of-bag (OOB) error rate and identification rate	The identification rate is 98%
[33]	Porcelain	Autocorrelation	Accuracy	90.7%
[76]	Polymer	stepwise regression	Accuracy	KNN is 57.5%, polynomial is 65%, and fuzzy is 56.3%
[77]	Porcelain	Discrete S transform	Accuracy	95% to 97%
[2]	Silicone rubber	stepwise regression, PCA, and moving average filter	Accuracy, RMSE	68% for four classes and 95% for two
[78]	Porcelain	STMHT and FLDA	Accuracy	90%
[79]	Porcelain	Extract distortions	Error	4% to 7%

Table 6. *Cont.*

Reference	Insulator Type	Preprocessing Stage	Metrics	Accuracy
[80]	Porcelain	Mathematical morphological function and statistical operations	Precision	100%
[81]	Glass	Data augmented using: Gaussian, Salt and Pepper, Poisson, and Speckle noise.	Accuracy	99.76%
[82]	Ceramic	Modelling current equation	MAPE	MAPE= 0.4%, for Imax = 1.292 mA
[83]	Ceramic	GLCM and Tamura features of the spectrograms	Accuracy and computational time	90.6%
[84]	Polymeric	Hyperbolic window Stockwell transform	Accuracy, sensitivity, and specificity	RF (=97.5%)
[85]	Porcelain	Data are standardized using the KMO test and Bartlett spherical test	MAE, RMSE, MAPE, mean squared percentage error (MSPE), Theil inequality coefficient (TIC), coefficient of determination (R2), modeling time (TM), and prediction time (TP)	MAPE is 1.567
[86]	Porcelain, glass, and polymer	FFT	Error	2%

4.2. The Imaging Method

In this section, various imaging methods will be discussed that are used for contamination level monitoring. Visual image analysis is a cost-effective method that does not require expensive imaging equipment or high relative humidity (RH). On the other hand, methods based on infrared (IR) and ultraviolet (UV) images are promising; however, they require relatively expensive equipment and high RH. In addition, the images are limited to specific bands, which limits the information acquired from the insulator surface. To cater to these limitations, hyperspectral technology is used to achieve multiband high-resolution images, thus combining the advantages of visible, IR, and UV bands; a comparison was tabulated in [87] and is reproduced in Table 7.

Table 7. Comparison of different detection conditions [87].

	Visible Light	Infrared	Ultraviolet
Temperature	-	≥5 °C 5 °C or higher	-
Relative humidity	-	≤85% 85% or less	-
Wind speed	≤5 m/s	≤0.5 m/s	≤1.5 m/s
Weather	The weather is sunny and should not be thunder, rain, fog, snow, etc.	The weather is cloudy, and it is advisable to avoid thunder, rain, fog, snow, etc.	Should not be thunder or heavy rain
Visibility	High	Relatively high	Relatively high
Best time	Daytime for surface shape test, night for partial discharge detection	At night, two hours after sunset	At night
Electromagnetic interference	-	Avoiding	Avoiding
Heat source radiation	-	Avoiding	-
Background radiation	-	Balance	-

Thermal imaging, which is used to determine if the insulator is at an acceptable temperature, has weaknesses because it depends on the amount of current that heats parts of the material or where spots can be detected using images. This method requires maintaining the correct distance and angle and specialized software for image analysis.

4.2.1. Digital Imaging Method

In [88], image-based contamination detection was reported for ZSW-10/4 insulators under different contamination levels, where the mean value of the V component in YUV color space was used to distinguish between contamination levels in terms of ESDD. A neural network (NN)-based detection system gave 90% testing accuracy for contamination level monitoring. Another NN-based study was reported in [10], which used linear algebraic features of HSV color space to correlate with ESDD. Similarly, in [1], both statistical and linear algebraic features of images were used to train a NN for contamination level detection. Very high detection performance was reported.

Due to several advantages of silicone rubber insulators, it is highly relevant to study the deterioration of these insulators as their performance is highly affected by severe contamination levels. In this spirit, image processing techniques were developed and reported in [89] for the assessment of silicone rubber insulator contamination. Textural and statistical features, such as discrete cosine, wavelet, Radon, contourlet transformation, gray-level co-occurrence matrices, and stepwise regression, were used. Moreover, the tested classifiers included k-nearest neighbor, neural networks, and linear classifiers. An accuracy of 96.5% was reported for seven hydrophobicity conditions using NN classification of the fused features.

The red, green, and blue (RGB) and hue, saturation, and value (HSV) images of 70 kN disc-type porcelain insulators in a laboratory setting were analyzed in [90], where the dust density was 5 times the salt density. The extracted features comprised mean, standard deviation, maximum, minimum, range, mode, median, kurtosis, and skewness. To determine the pollution level, cluster analysis was used. Another study for porcelain insulators [91] used images to classify NSDD. Four classifiers were used, namely Polynomial, NN, quadratic discriminant analysis (QDA), and adaptive neuro–fuzzy inference system (ANFIS), and their performances were compared. The highest accuracy was reported with ANN of 93.75%, and a minimum overall accuracy of 91% was recorded.

Field-polluted composite insulators were analyzed in [92] using the features of R, G, B, H, S, and V component images. Specifically, the S component features served as an input to support the vector machine for contamination grade classification. An accuracy of 97.5% was reported.

4.2.2. Thermal Image (Infrared, Thermal Vision)

In [93], both visible and infrared images were used to detect the fine details and large-scale edge information, respectively, using guided image processing. To decompose the image, a novel and efficient methodology based on latent low-rank representation (LatLRR) was introduced. The experiments were reported to show superior performance compared with the multiscale decomposition for insulator contamination level monitoring. In [94], infrared images were used to detect the contamination level on high-voltage insulators. Specifically, the images were processed by denoising and segmentation, and the features were extracted for radial basis function NN (RBFNN) to enhance the detection accuracy. Recently, photothermal radiometry (PTR) was used to classify pollution levels on ceramic discs in [95] in terms of ESDD and NSDD, where NaCl and Kaolin were used to emulate the soluble and nonsoluble contaminants. A multiclass semisupervised support vector machine was employed to cater to the nonavailability of labeled data. A direct relationship between contamination level, time, and frequency domain characteristics of thermal images and the high accuracy of the methodology were reported.

4.2.3. Ultraviolet Image

THD and fundamental components of UV signals were used as features for the NN in [96] to determine the contamination and aging levels of various insulators. The network was able to predict the flashover events on the basis of the discharge intensity levels. In [97], an accurate deep-learning-based contamination level predictor was designed, which used UV discharge images for a sparse autoencoder (SAE) and a deep belief network (DBN). Humidity and contamination levels varied while recording the UV spot area sequence for contamination recognition. The reported accuracy for three humidity levels of 80, 85, and 90% were 91.25%, 93.125%, and 92.5%, respectively. For ceramic insulators, a cost-effective UV sensor was employed to detect the contamination level in combination with texture analysis, time-frequency technique, and support vector machine (SVM) [83]. It was found that the combination of texture feature extraction methods with the SVM classifier gave an accuracy of 90.6%, which was far superior to a single time feature or other texture features. Another study of ceramic insulators was reported in [98], where a ceramic string consisting of 3 pieces of XWP-70 insulators was used. Four ESDD levels tested were 0.05, 0.1, 0.2, and 0.3 mg/cm^2 with fixed NSDD at 1.0 mg/cm^2. Curves for fuzzy logic inference were obtained by observing that the corona and partial arc discharge UV image areas and the number of discharge events are correlated with humidity and contamination severity.

A study involving combined features of IR and UV images of polluted ceramic insulators was given in [21] under humid conditions. PCA was used to obtain significant features, which were given to a particle swarm-optimized backpropagation neural network (PSO-BPNN) to distinguish between the contamination grades.

4.2.4. Hyperspectral Images

In [99], color information, hyperspectral spectral line characteristics, and image texture were combined as the detection basis for the classification algorithms. Compared with the model based on only spectral line features, the results of the fusion-based approach showed a detection accuracy of 95%. In the context of information fusion for contamination detection, [100] introduced a method that involved significant features selected out of 36 color and seven temperature features using visible and infrared images, respectively, which translated into high accuracy. No-dry, dry, and dry band arc heating models were numerically solved to theoretically evaluate the differences in temperature profiles depending on various operational conditions. Similarly, in [21], the fusion of infrared and UV image features based on PCA was reported to efficiently characterize contamination levels of artificially polluted ceramic insulators. The RH varied in the experiments with 80%, 85%, and 90% values. Similar to the previous works, the authors reported superior performance using combined infrared and UV images compared with using these features separately for each.

Another study based on the hyperspectral images of insulator contamination with soluble and nonsoluble contaminants was reported in [101]. The images were fed to a multiclassification model of extreme learning machine (ELM) to accurately classify the degree of pollution. Specifically, for different types of pollutants, the absorption peak, position of reflection peak, amplitude, and the change trend of the hyperspectral curve varied. However, only amplitude change was observed when the level of the same type of pollutant was varied. An accuracy of at least 95% was recorded for NaCl, CaSO4, and mixed NaCl-CaSO4. For silicone rubber coating of a composite insulator, [102] analyzed the hyperspectral images with both soluble and nonsoluble contaminations. The method based on combined multivariate scattering correction (MSC), successive projection algorithm (SPA), and linear discriminate analysis (LDA) gave the best classification performance. Table 8 shows the accuracy of using different types of images in detecting contamination levels.

Table 8. The accuracy of using different types of images in detecting contamination levels.

Reference	Insulator Type	Input Signal	Preprocessing Stage	Test Type (Dataset)	Metrics	Accuracy
[21]	Ceramic	IR and UV image	Fisher criterion and KPCA	Experiment-Field (120 samples for testing and 280 for training)	Accuracy	96.67%
[10]	Porcelain	Images	Matrix manipulation and edge-based segmentation	Experiment-Field (51 samples: 36 for training and 15 for testing)	Mean absolute error (MAE), predicting rate	MAE: 0–0.045 and predicting rate is 80%
[90]	Porcelain	Images	Denoising, image segmentation, and PCA	Experiment-Field (40 groups of samples)	Probability density	-
[103]	Porcelain	IR images	Flat shot to image test pieces, grayscale	Experiment-Lab (700 images: 560 for training and 140 for testing)	Accuracy	93%
[94]	Porcelain	IR image	Denoising technique based on MAP segmentation, estimation, and wavelet generic Gaussian distribution	Experiment-Lab	Accuracy and time	97.31%
[1]	Glass and porcelain	Images	RGB to grey, RGB to HSV, and SVD	Experiment-Lab (40 for training and 19 for testing)	MSE and accuracy	84.2%
[77]	Porcelain	Leakage current	Discrete S transform	Experiment-Lab	Accuracy	95% to 97%
[91]	Ceramic	Images	Template matching and grayscale histogram	Experiment-Lab (96 images: 24 for each level)	Accuracy	ANN = 93.75%
[101]	Silicone rubber	Hyperspectral images	multiplicative scatter correction and black-and-white correction	Experiment-Lab (120 sets for training and 120 sets for testing)	Accuracy	From 87.5% to 90%
[104]	Porcelain	IR images	Denoising and enhancing contrast	Experiment-field (300 frames)	Accuracy	100%
[92]	Silicone rubber	RGB and HSV images	Segmentation method based on randomized Hough transform, and Fisher criterion	Experiment-Lab (65 samples for light and 59 for heavy, and the ratio is 2:1 for training and testing)	Accuracy, precision, recall, and f-measure	97.5%
[97]	Ceramic	UV discharge images	The grayscale images were converted to binary images, all set to black, excluding the white pixels.	Experiment-Lab (320 samples for training and 160 for testing)	Accuracy	92%
[95]	Ceramic	Images	PCA	Experiment-Field (frame size of 640 × 512 pixels)	Accuracy	90%
[102]	Silicone rubber	Hyperspectral image	MSC, PCA, SPA	Experiment-Lab (176 variables)	Accuracy and Kappa	LDA (=97.5%)
[105]	Ceramic	Images	Bounding box	Experiment-Field (2973 images)	Mean average precision (mAP) and processing time	onshore: mAP is 0.67 and processing time is 0.55 s, onboard: mAP is 0.26 and processing time is 1.27 s
[106]	Polymeric	Audible (ultrasound) signal	wavelet transform (WT), filtering, and noise reduction	Experiment-Lab (20,000 samples: 70% for training and 30% for testing)	RMSE, MAPE, MAE, and R2	R2 is 0.9982
[107]	Porcelain	Discharge image	Grayscale, binarization, and main spot feature extraction on the image	Experiment-Field (1243 pictures: 994 for training and 249 for testing)	Accuracy	84.8%
[99]	Porcelain	Hyperspectral image	GGCM, color feature, and KPCA	Experiment-Lab (Ten sets for each pollution level: 20 for training and 20 for testing)	Accuracy	95.0%

Table 8. *Cont.*

			Gaussian filtering, Canny algorithm, edge location, and multiplicative scatter correction	Experiment-Lab (1200 samples with ratio of 7:3 for training and testing)	Accuracy	96.9%
[108]	Porcelain	Images				

4.3. Acoustic Emission (AE), Microwave & Ultrasonic

The precipitation of contaminants on the insulator surface is known as a prevalent cause of partial discharges (PD). In a practical sense, as the level of contamination rises, the severity of PD grows. The existence of PD produces acoustic noise that can be attained and compared with the contamination levels to predict the severity of pollution [109]. A study conducted an artificial pollution test to compare the contamination level with the acquired signal (PD noise). It was observed that the system produces reasonable indicators of the contamination level [110,111].

Contamination level monitoring methodologies based on LC, IR, or UV images give reliable results only when the contamination layer is dampened, whereby the occurrence of a flashover event might be premature, i.e., before the right time for cleaning or maintenance service. Moreover, in the case of LC, an additional disadvantage results from the installation of its measurement equipment which reduces insulation security [112]. An alternate method to determine the need for insulator maintenance is the perception of AE based on the experience of the network operators. Even with relatively low accuracy, it is an effective indicator of the risk of power system outages and for defining the maintenance actions in the search for the optimum time to clean insulators.

In [113], it was demonstrated that the frequency-related features of AE signals have a good correlation with the polluted insulator's corona, partial, and arc discharge. For glass insulators, wavelet transform was applied to extract contamination level information from the AE of corona discharge (CD) [114]. Salt-based pollution was simulated in a humid environment. It was reported that the wavelet transform could successfully differentiate between the background noise and AE due to CD, where both contain the same features. In [110], the pollution severity was correlated with the time and frequency domain characteristics of the AE signal, and the developed system was able to correctly identify the contamination level.

Besides AE, microwave and ultrasonic are other nonelectrical techniques used for the monitoring of contamination levels. Microwave nondestructive testing techniques can detect small thickness variations in dielectric layers and small variations in some dielectric properties in stratified dielectric composites because they can penetrate limited-loss dielectric materials and interact with their inner structure without being exceedingly attenuated [115,116].

In [112], the use of a 10.45 GHz microwave reflectometer was reported, whereby the power level of microwave energy reflected back from contaminated glass insulators under dry conditions was able to correctly differentiate between different contamination levels. The idea was that the electromagnetic energy reflected by a contaminated insulator is different from a clean insulator. The ESDD was varied from 0.02 to 0.15 mg/cm^2 and correctly differentiated by the developed technique.

In [106], ultrasound signals from in-service porcelain insulators were used to forecast the contamination levels. It was reported that the hybrid forecasting technique based on the combination of stacking ensemble learning model and wavelet transform outperformed adaptive neuro–fuzzy inference system (ANFIS) and long-term short-term memory (LSTM). Table 9 shows the accuracy of using different signal processing techniques for the acoustic signal in detecting contamination levels.

Table 9. The accuracy of using different signal processing techniques for acoustic signals in detecting contamination levels.

Reference	Insulator Type	Preprocessing Stage	Metrics	Accuracy
[117]	-	Bottom-Up segmentation, wavelet energy coefficient, principal component analysis,	Recall, precision, accuracy, time, and F-measure	98%
[118]	Glass	WPT	RMSE, MAE, R2	R2 for testing in grid partition is 0.9592
[106]	Polymeric	wavelet transform (WT), filtering, and noise reduction	RMSE, MAPE, MAE, and R2	R2 is 0.9982

4.4. Contact Angle

Contact angle (CA) measurement is performed to assess the hydrophobicity property (HP) of the insulating material and is used to quantify the wetting of a solid by a liquid. Increasing the contact angle of the water drop is a sign of improving the hydrophobicity.

In [16,119], the effect of contamination on the hydrophobic properties of silicone rubber was investigated, while [120,121] investigated the effect of algae contamination. In [122,123], the study was conducted after applying hydrophobic insulator coatings. The results showed that having less contact angle indicated poor hydrophobicity.

The insulators are coated with Silicone rubber in some cases. However, the HP of these coatings significantly deteriorates under humid conditions, which changes the CA of water droplets. In this spirit, [124] investigated Silicone coating performance under the influence of humidity with varying CA. Field samples of DC composite insulators in South China were tested in [125] to study their HP using the CA method and compare them with the samples without contamination. Moreover, hydrophobicity transfer with artificial contamination was also studied. It was observed that the middle part of the insulator outperformed the high- and low-voltage ends in terms of hydrophobicity and hydrophobicity transfer.

4.5. Partial Discharge (PD)

It was reported in [126] that the intensity, duration, and rise-time of the PD pulse increases significantly with an increase in surface wetness, regardless of the contamination level on the insulator surface. A relationship between RH and PD spectrum was given such that for RH values of 60% to 80%, most of the PD energy lay in the 6–25 MHz frequency range, whereas for higher RH (90% and above), the signal energy was focused more in 2–6 MHz range. The study was also extended to the case of polluted conditions, where the PD pulse duration increased with higher contamination levels. In [127], SIR insulators were studied for the occurrence of PD. It was observed that the low-frequency components (0–78 Hz) dominated the discharge signal's spectral content at any stage from initiation to complete discharge. In [128], it is reported that the discharge signals are proportional to the water conductivity, contamination level, and damage on the insulator surface.

5. HV Insulator Contamination Level Classification Techniques

The following sections summarize the work done in the last decade on HV insulator contamination level classification techniques.

5.1. Machine Learning

Neural network (NN) is a kind of machine learning, and it is also called artificial neural network (ANN), where the network employs complex mathematical models for data processing. NN connects a network of units called neurons, and the collection of these neurons constructs a network called a neural network. In addition to the neurons, NN contains links and weights, activation functions, layers, hyperparameters, learning rate, and cost function. Each ANN in the system consists of a set of layers with multiple neurons worked by using activation functions, and it is designed to be adjusted to a dynamic input.

Indeed, each neuron receives different versions of the input along with a weight value, and it is then added to a small value called bias. After that, it is passed to the activation function that determines the final output value.

5.1.1. Backpropagations Neural Network (BPNN)

Jin and Zhang [21] proposed a technique to figure out the contamination severity in the ceramic insulator based on the feature fusion of both the ultraviolet (UV) and infrared (IR) image information. After preprocessing the images, a Fisher criterion was applied to gain features of IR and UV images. For feature fusion, kernel principal component analysis (KPCA) was adopted to reduce the dimension of the generated features and obtain only a three-dimensional fused feature. These features were fed into a particle swarm-optimized backpropagation neural network (PSO-BPNN) classifier to realize the contamination grade. Paper [10] presented a developed intelligent technique for specifying the contamination level of high voltage (HV) insulators. Maraaba, Al-Hamouz et al. adopted two methods in the feature extraction stage to extract the main features from the insulator images. The first is matrix manipulation, and the second is edge-based segmentation. After that, the singular value decomposition (SVD) was applied to obtain the linear algebraic features. Then, a multilayer feed-forward neural network was fed with these features to predict the ESDD level of the insulator. He, Luo et al. [94] proposed a learning model based on the radial basis function neural network (RBFNN) and the collected infrared images from the porcelain insulators to define the contamination level. They used the first-order, second-order, and third-order color moments as the main features, along with the relative humidity for the detection process. Since RBFNN has many parameters that affect its accuracy and speed, they used the support vector regression technique to define the number of hidden centers. Another technique based on statistical analysis was used to determine the initially hidden centers. This improved learning model combined with the random number control factor and gradient descent algorithm to achieve higher accuracy with less time. In paper [1], Maraaba, Alhamouz et al. proposed a neural network model for predicting the contamination level of the HV glass and porcelain insulators. It indicates the contamination level without the requirement of the deposition of hydrophobic materials and depends on the captured images. They extracted two types of features based on singular value decomposition (SVD): linear algebraic features and histogram-based statistical features. Then, they constructed three neural network scenarios for testing one type of these features or both, and the output of the neural network was the contamination levels. In a paper [129], Al Khafaf and El-Hag presented a new learning model based on a Bayesian regularized neural network to predict the future values of the leakage current. They used the recorded leakage current signal, and they selected some components from the signal. These components were fed into the neural network to predict the future time series of both the fundamental and third harmonic of the leakage current.

Patel, Maarouf, et al. [91] proposed a technique of pollution level estimation that can be adopted on live lines with the use of pattern recognition and image processing technology. Template matching and grayscale histograms were used on the collected images to clean and extract the main features. Three classification methods were used (i.e., Quadratic discriminant analysis (QDA), polynomial, artificial neural network (ANN), and Leave-one-out cross-validation (LVOCV)) to predict the pollution level, and all of them achieved high classification accuracies. An intelligent contamination prediction model proposed in [130] is based on an optimized backpropagation (BP) neural network with a genetic algorithm (GA). Here, Jinlei, Chao, et al. used the genetic algorithm to make the learning model faster and more robust for any change. The extracted features that were used to feed the BP are temperature, precipitation, wind, relative humidity, and air quality index (AQI). And the output of the BP model is the equivalent salt deposit density (ESDD) and nonsoluble deposit density (NSDD). In [96], Suhaimi, Bashir et al. studied the UV signals' time and frequency components of the insulators under different contamination levels by using artificial neural networks (ANNs). The experimental studies showed that

there is a high correlation between the discharge intensity levels. Hence, this was used to extract the total harmonic distortion and fundamental frequencies from the signal. Then, the selected features were fed into the ANNs model to determine the flashover prediction with respect to the discharge intensity level of the insulator. In paper [131], Yan, Gang et al. designed a risk monitoring interface based on neural networks and fussy logic technologies for predicting the insulator flashover. It is constructed based on a trained backpropagation network to define the real-time state of the insulator. The input vector of the neural network was leakage current amplitude, relative humidity, and the ratio of the 3rd harmonic of the leakage current to the amplitude of the fundamental harmonic. In addition, the output of the neural network was the security state of the insulator linked to the fuzzy interface. They used three fuzzy subsets to represent the security state of the insulator (i.e., safe state, light alarm, and serious alarm). Liu, Yang, et al. [132] adopted the use of a backpropagation(BP) neural network in developing a local insulator pollution diagnosis device to provide a real-time diagnosis of the pollution in the insulators. This local insulator has the ability to communicate with the ultraviolet imager in real time. They used a set of parameters (i.e., apparent discharge, detection distance and gain, and photoelectron number) obtained from the ultraviolet imager as input of the BP neural network. The output of the BP neural network was the pollution level.

5.1.2. Support Vector Machine (SVM)

Zhao, Jiang, et al. [133] presented a new insulator technique for predicting the severity of the contamination level and avoiding any pollution flashover accidents. They used a set of features based on the environmental and experimental variables for finding the contamination level: relative humidity (RH), ambient temperature (T), leakage current (LC), namely the maximum pulse amplitude (Ih), the energy ratio (K), and the energy (E). Then, a variation from these features was obtained and fed to the least squares support vector machine (LS-SVM) model to define the level. Xia, Song, et al. [77] proposed a learning method that combines the S transform and the support vector machine (SVM) for classifying the contamination level of porcelain insulators. They used S transform in the feature extraction stage to extract the phase and the amplitude of each frequency point of the recorded leakage current signal. Hence, three main parameters (i.e., amplitude, phase, and total harmonic distortion (THD)) were selected as the input to the SVM model, and the output of the SVM was fed into four fuzzy subsets to determine the level. In this paper [134], Mahdjoubi, Zegnini, et al. improved the performance of the outdoor insulators by using an intelligent detection method based on the least square support vector machines (LS-SVM) learning strategy. They set the support vectors according to a quadratic Renyi criterion by adopting the training set. Insulator height, leakage length, insulator diameter, number of elements in the string, surface conductivity, and number of sheds were used as the input of the LS-SVM model, and the output was the flashover voltage. Here, the training data for this model were generated based on the finite element method. Abedini-Livari, Eshaghi-Maskouni, et al. in [19] discussed the partial discharge (PD) on polymeric insulators under different changes in the impact of physical defects, accelerated salt–fog aging process, and varying amounts of contamination. Here, they recorded the partial discharge of the insulators by using a UHF antenna. A wavelet packet tree was used in extracting the feature from the partial discharge signal. Then, the selected features (i.e., Skewness, kurtosis) were fed into a support vector machine (SVM) model to predict the condition of the insulator. Chen, Li et al. in [92] proposed a classifier based on a support vector machine and the color characteristic of visible images to predict the contamination level. They used an ellipse segmentation technique based on randomized Hough transform to extract the main feature from the visible images. So, around 36 types of characteristics of HSV and RGB components were extracted from the previous process. The mean and median of the S component were selected as the main features based on the Fisher criterion. These features were then fed into the support vector machine classifier to predict the contamination level. In a paper [95], Liu, Mei et al. presented a machine-learning technique based on a semisupervised support

vector and the use of photothermal radiometry (PTR) for predicting the contamination level. PTR was used in the measurement to define the pollution severity parameters: NSDD and ESDD on the transient and frequency thermal radiation characteristics of the contamination. Then, the main features were extracted, and their dimensions were reduced using principal component analysis (PCA). After that, a semisupervised classifier was fed with the remaining features to predict the contamination level based on a four classes problem. In paper [56], Sun, Zhang et al. proposed a learning model that combines the exploratory factor analysis (EFA) and the use of a support vector machine for predicting the contamination level of the insulators. They used EFA to minimize the factor variables, which could reduce the complexity of the model. Then, the selected factor variables were fed into the least squares support vector machine (LSSVM) to predict the contamination level. To achieve better results, they applied a nondominated sorting genetic algorithm II for defining the optimal LSSVM parameters. Results showed that the optimized EFA-LSSVM model outperforms the original LSSVM, multiple linear regression, and backpropagation neural network model in the model performance. Zhou and Chen [135] adopted the support vector machine model with data mining techniques to predict the flashover voltage under different gray and salt densities. The average value of the collected data points should not exceed 10%. The results showed that the support vector machine regression model improved the model performance in terms of error values and prediction accuracy, and it provided a reference for the measures of the insulators.

5.1.3. The k-Nearest Neighbours (KNN) Algorithm

Chaou, Mekhaldi, et al. [136] proposed a new method called recurrence quantification analysis (RQA), which has the ability to indicate the Recurrent Plot (RP) structures and to quantify the leakage current dynamics during the process. It was proposed to study the RP structures and leakage current dynamics and extract the main features from the current signals for detection purposes. Hence, eight RQA indicators were used to study and investigate the leakage current signals under different conductivities. After that, the mean values of the eight RQA indicators are considered as the input to KNN in order to predict the contamination severity.

Abouzeid, El-Hag, et al. [2] developed a nonintrusive method based on a machine learning technology to monitor and evaluate the silicone rubber insulators by predicting ESDD level. They used stepwise regression in the feature extraction stage and PCA to reduce the dimension of the extracted features from the leakage current. KNN was adopted to predict the ESDD level. In [102], Xia, Ren et al. proposed a new learning model based on hyperspectral imaging technology (HSI) for evaluating the high-temperature-vulcanized silicone rubber insulators. The Canny operator method was applied to the collected hyperspectral images to select the interesting areas and extract the spectral data. They also used a multivariate scattering correction (MSC) method to pre-treat the extracted data and PCA to reduce the dimension of the extracted features. Then, a successive projection algorithm (SPA) was applied to define the targeted bands. These bands were fed to KNN to predict the contamination level. Ma, Jin, et al. [83] proposed a new learning technique based on the texture features from the UV signals to predict the samples into local arcs, coronas, and long arcs. The texture analysis technique was adopted into the images obtained from the spectrograms of UV signals, and it was used to figure out the Tamura features and the grey-level co-occurrence matrix (GLCM). Then, the extracted features were fed to KNN to classify the partial discharge fault.

In [84], Sit, Das et al. presented an efficient method to predict the contamination level of the polymer insulators. They analyzed the leakage current in the time–frequency domain using hyperbolic window Stockwell transform (HST), and they extracted a two-dimensional complex time–frequency HS matrix. Then, they divided the HS matrix into magnitude and phase spectrum, and hence 16 features were extracted from the spectrum. Next, they used the least absolute shrinkage and selection operator (LASSO) method to select the best features (i.e., five features) from the extracted ones. The selected features were fed into

KNN to predict the contamination level. In [137], the KNN classifier based on insulator images is used for detecting contamination levels. The 40 porcelain insulators used in this study were artificially polluted. Six statistical features were extracted from insulator images and considered as inputs to the classifier, such as mean, variance, asymmetry, kurtosis, energy, and entropy. The classifier showed 85.17% accuracy using k-fold cross-validation. The accuracy of KNN was compared with other classifiers such as decision tree, ensemble subspace, and support vector machine and outperformed them.

5.1.4. Random Forests (RF)

In [75], Kannan, Shivakumar, et al. presented a machine learning technique based on a random forests (RF) classifier for classifying the contamination level of the HV insulators. A set of experiments was conducted, and the leakage current (LC) was recorded in the lab on the porcelain insulator at 11 kV AC voltage. They used the discrete wavelet transform technique and time-domain analysis to extract the histogram and basic features of the leakage current. Around 48 features were extracted from the current and then fed to the RF model in order to define the pollution severity. Ren, Li et al. [28] proposed a new learning technique for predicting the pollution severity of the insulators based on random forests (RFs). Moreover, they proposed 16 factors that are linked to the nonsoluble deposit density (NSDD) and equivalent salt deposit density (ESDD) for the learning process. Then, they adopted the mutual information (MI) theory for the feature extraction process based on the weights of the 16 factors. The regression model of RFs was constructed based on the extracted features and tested to predict the ESDD and NSDD levels and then compared with the result of the support vector machines (SVM) model. In [80], Sit, Chakraborty, et al. proposed a learning method based on the mathematical morphological function and the random forests classifier to classify the contamination level in the porcelain insulators. Leakage current was collected on different contamination levels from extensive experiments. They used different statistical operations and mathematical morphological functions in the feature extraction stage. Then, a different number of features (i.e., 1, 2, 3, and 21) was fed into the random forests classifier to predict the contamination level.

5.1.5. Ensemble Learning (EL)

Stefenon, Grebogi, et al. in [117] solved the faults in insulators as a multiclass problem using an ensemble extreme learning machine (EN-ELM) and particle swarm optimization. They applied 13.8 kV (rms) in contaminated, drilled, and good insulators and recorded the data using an ultrasound detector connected to a computer. They used wavelet energy coefficient, bottom-up segmentation, and principal component analysis in the feature extraction stage. The extracted features were fed into the optimized ensemble extreme learning machine to predict the class of contamination in the insulator. In paper [101], Qiu, Wu et al. proposed a detection technique based on the hyperspectral concept and machine learning technology. They collected samples from the hyperspectral images with different pollution levels by using a hyperspectrometer. Then, they used multiplicative scatter correction and black-and-white correction to correct the collected images. After that, they obtained from the corrected images the hyperspectral curves using the region of interest (ROI). The extracted features from these images were fed into a multiclassification model of extreme learning machine (ELM) to detect the pollution degree of the insulator. Stefenon, Ribeiro, et al. [59] proposed a learning model based on stacking ensemble in the prediction of polluted porcelain insulators. They used ultrasound equipment to record the signal and then a wavelet transform to filter the signal and remove the noise effects. The extracted signal was fed into a stacking ensemble model to predict the contamination of the insulator. A set of metrics was introduced in the results as mean absolute percentage error (MAPE), coefficient of determination (R2), and root means square error (RMSE). Yin, Xiao, et al. [61] presented a technique based on spectral characteristics and the hyperspectral image to detect the pollution degree in the insulators. They extracted image texture, characteristic color data, and hyperspectral spectral line characteristics of the insulator using the gray-

level gradient co-occurrence matrix (GGCM) and used kernel principal component analysis (KPCA) to reduce the dimension of the extracted features. Then, they fused the selected features to be used in the detection process. Next, the fused features were fed into an ensemble learning model to classify the sample into one of the four levels (i.e., light, medium, heavy, and very heavy).

5.1.6. Convolutional Neural Network (CNN)

A convolutional neural network (CNN) model was proposed in [103] for the diagnosis of the state of the porcelain insulators in the transmission lines. Liu, Pei, et al. used infrared image technology and then fed them to the LeNet CNN model; it was applied to optimize the network structure. The model showed a high classification rate, and it is robust and offers a better rate under different conditions such as humidity, temperature, thermal load, and position of deterioration on the insulator. In [104], a deep learning model was developed to find the zero-sequence insulators with different air humidity, contamination, and different locations. The authors used infrared images after removing the noise effect and increasing the contrast in the method. The output images were fed into a regional proposal network (RPN) and fast region-based CNN (RCNN) detection network for detecting the insulators. In [138], Feng, Xuran et al. proposed a deep learning model to locate and identify the defects of the insulators by the use of infrared images. They collected the infrared images and then filtered the interference of the background. Then, the cleaned images were fed into the multitarget detection algorithm YOLO for detecting the defects based on multifeature fusion. Once the defect is located in the infrared image, then the type of the defect is identified accordingly. In [81], Mussina, Irmanova, et al. proposed a fusion convolutional network (FCN) architecture for the evaluation of the contaminated outdoor HV insulators. FCN adopts the multimodal information fusion (MMIF) of UAV images with the leakage current and classifies the contamination of the insulator into conditions that are present before the failure, such as snow, water, salt, and metal dust. Using MMIF in the model reduced the complexity of the learning process and achieved better accuracy. In a paper [58], Waleed, Mukhopadhyay, et al. developed a drone-based system for monitoring the ceramic insulator on the power lines. The drone system is equipped with a Raspberry Pi single-board computer and onboard cameras to monitor the state of the insulators. The system also has the capability to perform some computer vision tasks related to the monitoring process; it can perform these tasks onboard or onshore at a ground station. In the case of onshore mode, the drone takes images and simultaneously transmits them to the ground station. Then, object detection methods (i.e., Single-Shot MultiBox Detector (SSD) Mobilenetv2) can be applied to classify the insulators into three levels: healthy, dirty, and broken insulators, while in the onboard mode, images were fed directly to region-based CNN (RCNN) to predict the level. In a paper [60], Liu, Lai, et al. proposed a convolutional neural network (CNN) model by using the discharge image to predict the pollution state of the insulators. They applied the binarization, grayscale, and main spot on the collected images in the feature extraction stage. Then, the extracted features were trained using a CNN model, and the pollution state was defined. The results showed that the discharge state of the insulators is positively correlated with humidity and surface pollution. In a paper [62], Zhao, Yan et al. proposed a learning model based on the hyperspectral technology for predicting the states in the porcelain insulators. They extracted the edges from the images using Gaussian filtering and the Canny algorithm to locate the cracks. Then spectral information was used to predict the state of the insulator by using the Efficient Net CNN model. The results showed that the achieved accuracy by using this model is 96%, which is better than other learning models and without the use of hyperspectral data. In a paper [139], Vigneshwaran, Maheswari, et al. proposed a learning model based on feature fusion and the dual-input VGG convolution neural network (CNN) for predicting the pollution severity of the insulator. The measured partial discharge signal was shaped as a time–frequency image named by a scalogram and 3D phase-resolved partial discharge (PRPD) patterns. The authors fed the dual-input CNN by the scalogram

and 3D PRPD patterns. Then, a weighting fusion method was used to select the best feature from the scalogram and 3D PRPD pattern features and to improve the recognition rate of the network. After extracting the features, the network was learned by adopting three different learning models based on the selected optimizer for the minimal loss function, i.e., root means square propagation (RMSPROP) optimizer, stochastic gradient descent with momentum (SGDM) optimizer, and adaptive momentum (ADAM) optimizer. Additionally, they used a Bayesian optimization for selecting the hyperparameters of the network.

5.2. Fuzzy

Fuzzy logic is introduced as many valued logic forms, and it contains multiple logical values of a variable between 0 and 1, which are partially true and partially false. Sometimes, humans cannot decide whether something is true or false in real life. Hence, the term fuzzy represents the things that are not obvious and not clear. A fuzzy algorithm gives the system some flexibility to find the best possible solution to the problem after considering all available information between the true and false values. The fuzzy logic algorithm has been used in different fields, from machine theory to artificial intelligence (AI), such as microcontrollers and workstation-based algorithms, for achieving the required output. It can also be executed in both software and hardware. In terms of HV insulators, three previous fuzzy logic approaches are discussed in this research.

In [98], Lu, Wang et al. studied the characteristic of the ceramic pollution discharge with the use of Ultraviolet (UV) images along with the artificial climate chamber. Based on the discharge UV image, they divided the discharge type into two types. The first one is the corona discharge (CDA), and the second is the partial arc discharge area (PDA) and partial arc discharge repetition (PDR). Then, a digital image processing algorithm was applied to the UV image for segmentation purposes, the number of the partial arc discharges at specific times was counted, and the correlation of the resulting variables with the relative humidity (RH) was found. After that, the fuzzy logic inference was used, where the correlated variables are the input, and the pollution grade is the output of the technique. Wang, Lin, et al. [140] used the mean of the leakage current and environment facts in a fuzzy logic system to define the pollution condition of the HV lines. They selected a set of parameters, such as the dew-point deficit, leakage current, wind speed, and relative humidity, to be the input of the fuzzy logic system after conducting data analysis. The output of the system is pollution level, and it was linked to a webpage service. Petri, Moutinho, et al. [141] presented a method for evaluating the state of the insulators based on the severity degree generated by an instrument. The instrument consists of two main parts, the first one is the algorithm's part, such as a fuzzy inference system or convolutional network, and the second part is the Raspberry Pi board. This instrument gives a range of severity degrees from 0 to 10, which indicates partial discharge activity. This degree was obtained using Mamdani fuzzy inference system and the extracted parameters from the partial discharge signals.

5.3. Nero Fuzzy

Lu, Yu et al. [142] proposed a new contamination detection technique based on a fuzzy neural network technology to overcome the drawback of the traditional detection techniques. They considered the characteristics of leakage current, relative humidity, and temperature while building the technique. Hence, as the input variables, the neural network included virtual value (Fl), leakage current peak value (Fp), temperature (T), leakage current pulse frequency (Ff), and humidity (H), and the weights of this network were constructed during the training process. The equivalent salt deposit density (ESDD), nonsoluble deposit density (NSDD), and hydrophobicity classification (HC) are the outputs of this network. In a paper [76], Khaled, El-Hag, et al. proposed a learning process for predicting the ESDD contamination level on the polymer insulators based on the recorded leakage current signals. After that, they used the stepwise regression method in the feature extraction stage and selected a set of features based on this method to feed to the learning

model: salt–fog conductivity, insulator length, voltage stress, leakage current peak value for 5 h, rate of change of peak value, rate of change of average peak value, and leakage current peak value for 15 min. Then, the authors fed these features to different classifiers: KNN, polynomial, and neuro–fuzzy classifiers to specify the contamination level based on the resulting ESDD range. They also found that when they reduced the classification problem from four classes to three classes, the recognition rate increased from 65% to 78% in the polynomial classifier. In [143], Salem, Abd Rahman, et al. proposed an artificial intelligence (AI) method which combines an artificial neural network (ANN) and adaptive neuro–fuzzy inference system (ANFIS) for predicting the voltage of the pollution flashover. Data used in this method were collected from the experimental works, and the theoretical results were generated from a validated model. Diameter D, form factor F, height H, equivalent salt deposit density (ESDD), creepage distance L, and flashover voltage correction (C) are the features that were used to train the AI network for predicting the voltage values.

Frizzo Stefenon, Zanetti Freire, et al. [118] proposed an offline time series forecasting method with an adaptive neuro–fuzzy inference system (ANFIS) to predict the insulator fault. They collected signals from the insulators using an ultrasound device. Then, they used a wavelet packet transform (WPT) to remove the noise effect in the collected signal and improve the efficiency of the time series forecasting process. They fed the extracted data into three system structures: fuzzy c-means clustering, subtractive clustering, and grid partition. They found that the wavelet neuro–fuzzy system with c-means clustering achieved the best accuracy compared with other structures.

5.4. Detrended Fluctuation Analysis (DFA)

In [144], Singh et al. used the detrended fluctuation analysis (DFA) on the recorded leakage current to predict the contamination level of the insulators. They observed that the DFA variable follows a specific behavior with the contamination level or the NaCl. Hence, this behavior was used to classify the contamination level, and this method showed the ability to remove the noise effect in the leakage current signal. Deb, Das, et al. [79] proposed a method for assessing the outdoor insulators based on the recorded leakage current and the use of detrended fluctuation analysis (DFA). They extracted the distortions from the recorded leakage current using a developed tracker signal based on the fundamental component; the authors found that these distortions give an indication of the contamination level of the tested insulator. Dey, Dutta, et al. [145] proposed a method based on the detrended fluctuation analysis (DFA) of the recorded leakage current to define the contamination level of the insulator. They used NaCl, Kaolin, and water to emulate the pollutant layer in the 11 kV suspension insulator disc. They showed that the DFA parameter gives a good indication of the level with respect to ESDD and conductivity.

5.5. Miscellaneous Techniques

Banik, Dalai, et al. [33] proposed a rough set theory (RST)-based method for classifying the contamination level of the porcelain insulators. These insulators were contaminated by the solid layer method (SLM) based on IEC60507, and the leakage current of the insulators was recorded for different levels and at different humidity values. Then, they used the autocorrelation concept for the feature selection process from the recorded leakage current since it is perfect for nonstationary leakage current and it has the ability to remove the effect of the noise in the current signal. After that, RST was applied to the extracted features to specify the contamination level of the insulator. In paper [78], Deb, Choudhury, et al. proposed a technique for predicting the contamination level on the HV lines based on the use of short-time modified Hilbert transform (STMHT) and sparse representation-based classification. They used STMHT and Fischer linear discriminant analysis (FLDA) in the feature extraction and feature reduction stages based on the recorded leakage current signals. The selected features were peak, mean, standard deviation, charge, and crest factor. These features were fed into the sparse representation-based classification model to predict the contamination level. In [93], Yan, Duan et al. proposed a method called latent low-rank

representation (LatLRR) for image fusion. They collected the infrared and visible images of insulators from the HV substations under normal operation. Then, they preprocessed the visible images by guiding and filtering the images to preserve edge information in the images. This method showed that it has the ability to extract the temperature information from the infrared image so as to define the state of the insulator in the infrared image and keep the texture details of the visible image in the fusion image. So, the remaining information in the fusion image will define the contamination of the insulator. Liao, Li et al. in [146] used the technology of laser-induced breakdown spectroscopy system (LIBS) along with principal component analysis (PCA) to predict the contamination level of the insulator. The laser system was used to bombard the natural and artificial contaminated insulators with different contamination levels. The authors used a camera and spectrometer to collect the emission spectrum. The peak of the spectral line was used in specifying the element types, and then the PCA was used for classifying the spectral line into four contamination levels. In [25], de Santos and Sanz-Bobi proposed a method for predicting the leakage current of the insulator while considering the weather and environmental information of the insulator's location. They developed a Cumulative Pollution Index (CPI) to find the soluble pollution deposit value on the insulator. The resulting value, along with wind, directional dust, and rain data, were learned using the random forests algorithm in order to determine the leakage current in the RTV silicone-coated insulators and toughened glass. In [147], Ahmad, Tahir, et al. presented a learning method for predicting the flashover parameters in the silicone rubber insulators under different values of ESDD, NSDD, humidity, and temperature. Data were collected from experimental works in the lab under controlled conditions. Four parameters and their effect on flashover voltage, arc inception, and surface resistance were studied. Cleaned data from the four parameters were trained using different learning models such as decision tree (DT), artificial neural network (ANN), least squares boosting ensemble (LSBE), polynomial support vector machine (PSVM), and Gaussian SVM (GSVM). In addition, to improve the accuracy of the model, the authors used the bootstrapping technique to increase the sample space. Zhang and Chen [97] presented a deep learning model based on the use of a deep belief network (DBN) and a sparse autoencoder (SAE) for predicting the contamination grade in the insulator. They used a double-layer stacked SAE to extract the spare features from the ultraviolet discharge images. Then, the extracted features were trained using DBN, which consists of three layers of restricted Boltzmann machine (RBM), to predict the contamination grade. Palangar and Mirzaie [148] proposed a technique for predicting the critical conditions in the glass and porcelain insulators using the leakage current. They defined a new index called by phase index; it represents the cosine of the phase angle of fundamental harmonics of the current. Based on the index, when the value is lower than 30%, the insulator is considered in an efficient state, and there is no flashover. On the other hand, when the index is higher than 30%, the insulator is put under investigation. Additionally, the authors found that when the humidity increases, the index increases accordingly. In paper [149], an innovative method was proposed to evaluate the risk of uniform and nonuniform pollution and wet glass insulator. Salem, Abd-Rahman, et al. proposed an alternative index to estimate the risk of the insulator, called Rhi, which is constructed based on the third, fifth, and seventh harmonic components of the leakage current. They tested the new index experimentally under different contamination conditions and estimated the risk of the insulator using normal and probability distribution functions (PFD). Moreover, they studied the impacts on the degree of flashover occurrence probability and the flashover voltage gradient.

Ibrahim and Abd-Elhady [55] proposed a monitoring method for pin-type and cap and pin-type HV insulators. The method depends on the use of a low-cost Rogowski coil transducer that fits around the pin of the insulator. They analyzed the output voltage from the coil winding by using fast Fourier transform (FFT). Based on the obtained spectrum, the pollution level of the insulator can be defined directly. It was validated and tested using an experimental setup by recording the voltage and leakage current and then finding the pollution level from their spectrum using the FFT analysis. In [150], Wahyudi, Setiawan

et al. investigated the ultraviolet (UV) released by a partial discharge that occurred in the dry and polluted conditions of the insulators. The intensity and UV image were recorded for one minute per voltage change per pollutant weight change, and the voltage stress was varied until the flashover happened. It was observed that there was a fixed relation between the UV emission parameters and the pollutant weight. In addition, it was noted that the UV intensity has three main values—minimum, maximum, and average—and they fluctuated in the recording stage. Based on these values, the authors showed that there were two UV-image patterns that could be identified: concentrated light and scattered points. The higher UV intensity means a higher deviation between the minimum and maximum values, and the highest concentrated light pattern was defined during a critical condition. Salem, Abd-Rahman, et al. [26] presented an innovative and alternative method to predict the pollution level of the HV insulator based on the higher component up to the seventh component of the leakage current. They formulated the new harmonic index based on the ratio of the sum of the seventh and fifth components to the third harmonic component. Next, they recorded the leakage current using a shunt resistor and current transformer. Then, a set of lab tests was conducted on porcelain and glass insulators under a salt–fog pollution state, and they are represented by three levels: light, high, and medium contamination. In a paper [151], Banik, Nielsen, et al. studied the effect of the distorted supply voltage on the leakage current of the silicone rubber insulators. They found that the supply voltage distortion causes an impact on the measured leakage current as in relative humidity and contamination severity. Hence, they proposed a crest factor-based leakage current analysis method to predict the pollution level of the insulator under distorted supply voltages. Based on the crest method, four clusters were identified with respect to the crest factor values of different insulators. Those clusters were used to define the severity level of the silicone rubber insulator.

Castillo-Sierra, Oviedo-Trespalacios, et al. [82] presented a method for predicting and monitoring the leakage current of the polluted insulator to define the suitable washing date. The exponentially weighted moving average (EWMA) control chart was used to specify the suitable days for washing the insulator so that the washing omissions and false alarms could be reduced.

6. Conclusions

This paper has reviewed the different methods adopted to identify the contamination levels in high-voltage insulators. Various techniques have been discussed alongside their advantages and disadvantages based on the published research work in the last decade. The major high-voltage insulator contamination level classification techniques discussed include machine learning, fuzzy logic, neuro–fuzzy interface, detrended fluctuation analysis (DFA), and various other techniques. However, each of these major categories includes various methods which have been proposed by different researchers and have been discussed throughout this work. The insulator contamination and the sources of contaminants have also been discussed. Moreover, the different methods of improving insulator performance in the industry have been analyzed. It has been noted that different techniques, such as coating, creepage extenders, optimization of electric field distribution, and cleaning, are being used by the power utilities to improve the insulators' performance. For instance, it has been noted that adding hydrophobic material on the surface of insulators improves the performance of ceramic insulators, such as the use of high-temperature-vulcanized silicone rubber (HTV-SiR) and room-temperature-vulcanized silicone (RTV-SiR) which offer better characteristics in terms of high tensile strength, better curing, easy processing, actuation, compressive mechanical behavior, and better hydrophobicity, among other silicone rubbers. Furthermore, it has been noted that the coated insulator has less leakage current compared with the noncoated insulator at the same voltage level. The use of the leakage current magnitude as a gauge for the pollution severity on the insulation has been analyzed by reviewing different methods. It has been observed that when mathematical morphological function and statistical operations are used in the preprocessing stage to test porcelain

insulator, the highest accuracy of 100% is obtained while the lowest accuracy (2%) is achieved when FFT signals are used to test the porcelain, glass, and polymer insulators. Hence, it is expected that this work will act as a reference guide for power utilities and researchers to select the best methods for contamination level identification based on their effectiveness and economic feasibility.

References

1. Maraaba, L.; Alhamouz, Z.; Alduwaish, H. A neural network-based estimation of the level of contamination on high-voltage porcelain and glass insulators. *Electr. Eng.* **2018**, *100*, 1545–1554. [CrossRef]
2. Abouzeid, A.K.; El-Hag, A.; Assaleh, K. Equivalent salt deposit density prediction of silicone rubber insulators under simulated pollution conditions. *Electr. Power Compon. Syst.* **2018**, *46*, 1123–1133. [CrossRef]
3. Kim, T.; Yi, J. Application of hydrophobic coating to reduce leakage current through surface energy control of high voltage insulator. *Appl. Surf. Sci.* **2022**, *578*, 151820. [CrossRef]
4. Kalla, U.K.; Suthar, R.; Sharma, K.; Singh, B.; Ghotia, J. Power quality investigation in ceramic insulator. *IEEE Trans. Ind. Appl.* **2017**, *54*, 121–134. [CrossRef]
5. Gençoğlu, M.T. The comparison of ceramic and non-ceramic insulators. *Eng. Sci.* **2007**, *2*, 274–294.
6. Patel, C.R.; Patel, N.; Patel, R. Condition Assessment of Silicon Rubber Insulator used in Overhead Systems. In Proceedings of the 2020 21st National Power Systems Conference (NPSC), Gandhinagar, India, 17–19 December 2020; pp. 1–5.
7. Rajini, H.; Ballaji, A.; Saahithi, S.; Bharat, M.; Ashwini Kumari, P.; Raghu, C. Comparative performance of insulating materials used in high voltage insulators. *AIP Conf. Proc.* **2022**, *2461*, 040001.
8. Saleem, M.Z.; Akbar, M. Review of the performance of high-voltage composite insulators. *Polymers* **2022**, *14*, 431. [CrossRef] [PubMed]
9. Maraaba, L.S.F. *Image Processing Based Contamination Level Monitdoring of High Voltage Insulator*; King Fahd University of Petroleum and Minerals: Dhahran, Saudi Arabia, 2013.
10. Maraaba, L.; Al-Hamouz, Z.; Al-Duwaish, H. Prediction of the levels of contamination of HV insulators using image linear algebraic features and neural networks. *Arab. J. Sci. Eng.* **2015**, *40*, 2609–2617. [CrossRef]
11. Gorur, R.; Sivasubramaniyam, S. Computation of defect-induced electric fields on outdoor high voltage ceramic and non-ceramic insulators. In Proceedings of the Annual Report Conference on Electrical Insulation and Dielectric Phenomena, Cancun, Mexico, 20–24 October 2002; pp. 319–322.
12. Kiessling, F.; Nefzger, P.; Nolasco, J.F.; Kaintzyk, U. *Overhead Power Lines: Planning, Design, Construction*; Springer: Berlin/Heidelberg, Germany, 2003; Volume 759.
13. Baker, A.; Farzaneh, M.; Gorur, R.; Gubanski, S.; Hill, R.; Karady, G.; Schneider, H. Insulator selection for AC overhead lines with respect to contamination. *IEEE Trans. Power Deliv.* **2009**, *24*, 1633–1641. [CrossRef]
14. Rizk, F.A.; Trinh, G.N. *High Voltage Engineering*; CRC Press: Boca Raton, FL, USA, 2018.
15. Alyousef, Y.; Varnham, A. Saudi Arabia's National Energy Efficiency Programme: Description, achievements and way forward. *Int. J. Low Carbon Technol.* **2010**, *5*, 291–297. [CrossRef]
16. Maraaba, L.S.; Al Soufi, K.Y.; Alhems, L.M.; Hassan, M.A. Performance evaluation of 230 kV polymer insulators in the coastal area of Saudi Arabia. *IEEE Access* **2020**, *8*, 164292–164303. [CrossRef]
17. Khattak, A.; Alahamdi, A.A.; Iqbal, M.B. Degradation Performance Investigation of Hydrothermally Stressed Epoxy Micro and Nanocomposites for High Voltage Insulation. *Polymers* **2022**, *14*, 1094.
18. Sk, M.H.; Ardila-Rey, J.A.; Umar, Y.; Mas'ud, A.A.; Muhammad-Sukki, F.; Jume, B.H.; Rahman, H.; Bani, N.A. Application and Suitability of Polymeric Materials as Insulators in Electrical Equipment. *Energies* **2021**, *14*, 2758.
19. Abedini-Livari, A.; Eshaghi-Maskouni, M.; Vakilian, M.; Firuzi, K. Line Composite Insulators Condition Monitoring through Partial Discharge Measurement. In Proceedings of the 2019 International Power System Conference (PSC), Tehran, Iran, 9–11 December 2019; pp. 595–600.
20. Arief, S.; Abral, H.; Hazmi, A.; Waldi, E.; Ahmad, M. Estimated leakage current based on the thermal image of the polymer insulator using the color detection method. *J. Physics Conf. Ser.* **2019**, *1317*, 012025.

21. Jin, L.; Zhang, D. Contamination grades recognition of ceramic insulators using fused features of infrared and ultraviolet images. *Energies* **2015**, *8*, 837–858. [CrossRef]
22. Han, S.; Hao, R.; Lee, J. Inspection of insulators on high-voltage power transmission lines. *IEEE Trans. Power Deliv.* **2009**, *24*, 2319–2327. [CrossRef]
23. Kunicki, M.; Cichoń, A. Application of a phase resolved partial discharge pattern analysis for acoustic emission method in high voltage insulation systems diagnostics. *Arch. Acoust.* **2018**, *43*, 235–243.
24. Pernebayeva, D.; Irmanova, A.; Sadykova, D.; Bagheri, M.; James, A. High voltage outdoor insulator surface condition evaluation using aerial insulator images. *High Volt.* **2019**, *4*, 178–185. [CrossRef]
25. de Santos, H.; Sanz-Bobi, M.Á. A Cumulative Pollution Index for the Estimation of the Leakage Current on Insulator Strings. *IEEE Trans. Power Deliv.* **2020**, *35*, 2438–2446. [CrossRef]
26. Salem, A.A.; Abd-Rahman, R.; Al-Gailani, S.A.; Kamarudin, M.S.; Ahmad, H.; Salam, Z. The leakage current components as a diagnostic tool to estimate contamination level on high voltage insulators. *IEEE Access* **2020**, *8*, 92514–92528. [CrossRef]
27. Salam, M.A.; Aamer, K.; Hamdan, A.; Hamdan, N. Study the Relationship between the Resistance and ESDD of A Contaminated insulator A Laboratory Approach. In Proceedings of the Proceedings of the 7th International Conference on Properties and Applications of Dielectric Materials (Cat. No. 03CH37417), Nagoya, Japan, 1–5 June 2003; pp. 1032–1034.
28. Ren, A.; Li, Q.; Xiao, H. Influence analysis and prediction of ESDD and NSDD based on random forests. *Energies* **2017**, *10*, 878. [CrossRef]
29. Montoya, G.; Ramirez, I.; Montoya, J. Correlation among ESDD, NSDD and leakage current in distribution insulators. *IEE Proc. Gener. Transm. Distrib.* **2004**, *151*, 334–340. [CrossRef]
30. Gorur, R.S.; Cherney, E.A.; Burnham, J.T. *Outdoor Insulators*; Ravi S. Gorur: Phoenix, AZ, USA,, 1999.
31. *IEC TS 60815-1*; Selection and Dimensioning of High-voltage Insulators Intended for Use in Polluted Conditions-Part 1: Definitions, Information and General Principles. International Electrotechnical Commission: Worcester, MA, USA,, 2008.
32. Banik, A.; Pradhan, A.; Ghosh, R.; Dalai, S.; Chaterjee, B. A comparative study on leakage current harmonics of porcelain disc insulator contaminated with NaCl and KCl. In Proceedings of the 2015 1st Conference on Power, Dielectric and Energy Management at NERIST (ICPDEN), Arunachal Pradesh, India, 10–11 January 2015; pp. 1–4.
33. Banik, A.; Dalai, S.; Chatterjee, B. Autocorrelation aided rough set based contamination level prediction of high voltage insulator at different environmental condition. *IEEE Trans. Dielectr. Electr. Insul.* **2016**, *23*, 2883–2891. [CrossRef]
34. Slama, M.E.A.; Krzma, A.; Albano, M.; Haddad, A.M. Experimental study and modeling of the effect of ESDD/NSDD on AC flashover of SiR outdoor insulators. *Energies* **2022**, *15*, 3782. [CrossRef]
35. Salem, A.A.; Lau, K.Y.; Abdul-Malek, Z.; Al-Gailani, S.A.; Tan, C.W. Flashover voltage of porcelain insulator under various pollution distributions: Experiment and modeling. *Electr. Power Syst. Res.* **2022**, *208*, 107867. [CrossRef]
36. Volpov, E.; Kishcha, P. Advanced modeling and mapping of severe pollution stress required for outdoor insulation coordination. *Electr. Eng.* **2022**, *104*, 741–752. [CrossRef]
37. Liu, L.W.; Thành, S.N. Towards the Feasibility of Long Range Wireless Power Transfer over an Ocean Surface. *Appl. Sci.* **2022**, *12*, 8751. [CrossRef]
38. Ullah, I.; Akbar, M.; Khan, H.A. Degradation analysis of RTV-SiR based composites under both polarities DC voltage for insulators coating. *Mater. Today Commun.* **2021**, *29*, 102890. [CrossRef]
39. Cherney, E.; Gorur, R. RTV silicone rubber coatings for outdoor insulators. *IEEE Trans. Dielectr. Electr. Insul.* **1999**, *6*, 605–611. [CrossRef]
40. Suwarno; Basuki, A. Mitigation of outdoor insulators failure using silicone coating. In Proceedings of the 2011 International Conference on Electrical Engineering and Informatics, Bandung, Indonesia, 17–19 July 2011.
41. Siderakis, K.; Pylarinos, D.; Thalassinakis, E.; Vitellas, I.; Pyrgioti, E. Pollution maintenance techniques in coastal high voltage installations. *Eng. Technol. Appl. Sci. Res.* **2011**, *1*, 1–7. [CrossRef]
42. Qing, Y.; Sima, W.; Jiazhuo, D.; Tao, Y.; Lin, C. New optimization method on electric field distribution of composite insulator. In Proceedings of the 2010 Annual Report Conference on Electrical Insulation and Dielectic Phenomena, West Lafayette, IN, USA, 17–20 October 2010; pp. 1–4.
43. Karady, G.G.; Shah, M.; Brown, R. Flashover mechanism of silicone rubber insulators used for outdoor insulation-I. *IEEE Trans. Power Deliv.* **1995**, *10*, 1965–1971. [CrossRef]
44. Vlastos, A.E.; Sherif, E. Natural ageing of EPDM composite insulators. *IEEE Trans. Power Deliv.* **1990**, *5*, 406–414. [CrossRef]
45. Al-Hamoudi, I.Y.; Al-Hamouz, Z.M. Field and laboratory performance evaluation of SiR insulators in the eastern coastal area of Saudi Arabia. In Proceedings of the 2004 IEEE International Conference on Solid Dielectrics, ICSD 2004, Toulouse, France, 5–9 July 2004; pp. 359–362.
46. Al-Hamoudi, I.; Al-Hamouz, Z. Reliability and cost effectiveness of silicone rubber insulators in the eastern coastal industrial area of Saudi Arabia. In Proceedings of the 2003 IEEE 10th International Conference on Transmission and Distribution Construction, Operation and Live-Line Maintenance, 2003 IEEE ESMO, Orlando, FL, USA, 6–10 April 2003; pp. 156–168.
47. Maraaba, L.; Al-Hamouz, Z.; Al-Duwaish, H. Estimation of high voltage insulator contamination using a combined image processing and artificial neural networks. In Proceedings of the 2014 IEEE 8th International Power Engineering and Optimization Conference (PEOCO2014), Langkawi, Malaysia, 24–25 March 2014; pp. 214–219.

48. Sopelsa Neto, N.F.; Stefenon, S.F.; Meyer, L.H.; Ovejero, R.G.; Leithardt, V.R.Q. Fault prediction based on leakage current in contaminated insulators using enhanced time series forecasting models. *Sensors* **2022**, *22*, 6121. [CrossRef]

49. Ghiasi, Z.; Faghihi, F.; Shayegani-Akmal, A.A. Artificial Neural Network Approach for Prediction of Leakage Current of polymeric insulator under Non-Uniform Fan-shaped Contamination. *Electr. Power Syst. Res.* **2022**, *209*, 107920. [CrossRef]

50. Richards, C.; Renowden, J. Development of a remote insulator contamination monitoring system. *IEEE Trans. Power Deliv.* **1997**, *12*, 389–397. [CrossRef]

51. Li, J.; Sun, C.; Sebo, S. Humidity and contamination severity impact on the leakage currents of porcelain insulators. *IET Gener. Transm. Distrib.* **2011**, *5*, 19–28. [CrossRef]

52. Mizuno, Y.; Nakamura, H.; Naito, K. Dynamic simulation of risk of flashover of contaminated ceramic insulators. *IEEE Trans. Power Deliv.* **1997**, *12*, 1292–1298. [CrossRef]

53. Jolly, D. *Dynamic Theory of Discharge Growth over Contaminated Insulator Surfaces*; IEEE Paper C; IEEE: New York, NY, USA, 1974.

54. Pei, C.; Shu, N.; Li, L.; Wang, D.; Li, Z. An acoustic emission method for on-line monitoring the contamination-causing flashover of insulator. In Proceedings of the 2008 International Conference on Electrical Machines and Systems, Vilamoura, Portugal, 6–9 September 2008; pp. 817–822.

55. Ibrahim, M.E.; Abd-Elhady, A.M. Rogowski Coil Transducer-Based Condition Monitoring of High Voltage Insulators. *IEEE Sens. J.* **2020**, *20*, 13694–13703. [CrossRef]

56. Jin, L.; Xu, Z.; Zhang, S. A pre-warning method of contamination flashover based on the leakage current of insulators in dry condition. In Proceedings of the 2017 International Symposium on Electrical Insulating Materials (ISEIM), Toyohashi City, Japan, 11–15 September 2017; pp. 757–760.

57. Deb, S.; Ghosh, R.; Dutta, S.; Dalai, S.; Chatterjee, B. Effect of humidity on leakage current of a contaminated 11 kV Porcelain Pin Insulator. In Proceedings of the 2017 6th International Conference on Computer Applications In Electrical Engineering-Recent Advances (CERA), Roorkee, India, 5–7 October 2017; pp. 215–219.

58. Chakraborty, S.; Podder, S.; Deb, S.; Nath, S. Qualitative Analysis of Contamination Severity between NaCl and CuSO 4 for Outdoor Insulator. In Proceedings of the 2018 IEEE Applied Signal Processing Conference (ASPCON), Kolkata, India, 7–9 December 2018; pp. 342–345.

59. Kordkheili, H.H.; Abravesh, H.; Tabasi, M.; Dakhem, M.; Abravesh, M.M. Determining the probability of flashover occurrence in composite insulators by using leakage current harmonic components. *IEEE Trans. Dielectr. Electr. Insul.* **2010**, *17*, 502–512. [CrossRef]

60. Patel, K.; Parekh, B. Prediction of flashover of silicone rubber insulator under different contaminated surface conditions. In Proceedings of the 2013 IEEE 1st International Conference on Condition Assessment Techniques in Electrical Systems (CATCON), Kolkata, India, 6–8 December 2013; pp. 358–361.

61. Zhengfa, L.; Qing, Z.; Wuyang, Z.; Shimian, L.; Gaolin, W.; Jianlin, H.; Maoqiang, B. Study on leakage current characteristics and influence factors of 110kV polluted composite insulators. In Proceedings of the 2018 12th International Conference on the Properties and Applications of Dielectric Materials (ICPADM), Xi'an, China, 20–24 May 2018; pp. 896–900.

62. Wang, J.; Gubanski, S.M.; Blennow, J.; Atarijabarzadeh, S.; Stromberg, E.; Karlsson, S. Influence of biofilm contamination on electrical performance of silicone rubber based composite materials. *IEEE Trans. Dielectr. Electr. Insul.* **2012**, *19*, 1690–1699. [CrossRef]

63. Li, J.; Sun, C.; Sima, W.; Yang, Q. Stage pre-warning based on leakage current characteristics before contamination flashover of porcelain and glass insulators. *IET Gener. Transm. Distrib.* **2009**, *3*, 605–615. [CrossRef]

64. Li, J.; Sima, W.; Sun, C.; Sebo, S.A. Use of leakage currents of insulators to determine the stage characteristics of the flashover process and contamination level prediction. *IEEE Trans. Dielectr. Electr. Insul.* **2010**, *17*, 490–501. [CrossRef]

65. Um, C.-G.; Jung, C.-G.; Han, B.-G.; Song, Y.-C.; Choi, D.-H. A fuzzy framework for flashover monitoring. In Proceedings of the International Conference on Fuzzy Systems and Knowledge Discovery, Changsha, China, 27–29 August 2005; pp. 989–993.

66. Mao, Y.; Guan, Z.; Wang, L. Analysis of the leakage current pulses of outdoor insulators in different relative humidity. In Proceedings of the 2007 Annual Report-Conference on Electrical Insulation and Dielectric Phenomena, Vancouver, BC, Canada, 14–17 October 2007; pp. 400–403.

67. Wang, J.; Xi, Y.; Fang, C.; Cai, L.; Wang, J.; Fan, Y. Leakage current response mechanism of insulator string with ambient humidity on days without rain. *IEEE Access* **2019**, *7*, 55229–55236. [CrossRef]

68. Amini, M.A.; Sedighi, A.R. A new procedure for determination of insulators contamination in electrical distribution networks. *Int. J. Electr. Power Energy Syst.* **2014**, *61*, 380–385. [CrossRef]

69. Amini, M.; Anaraki, A.S.; Sadeghi, M. High frequency components of feeder current as diagnostic tool to study contamination conditions of outdoor insulators in power distribution networks. In Proceedings of the 2013 21st Iranian Conference on Electrical Engineering (ICEE), Mashhad, Iran, 14–16 May 2013; pp. 1–6.

70. Algeelani, N.A.; Piah, M.A.M. Characterization of leakage current on high voltage glass insulators using wavelet transform technique. In Proceedings of the 2012 4th International Conference on Intelligent and Advanced Systems (ICIAS2012), Kuala Lumpur, Malaysia, 12–14 June 2012; pp. 882–885.

71. Kumagai, S.; Yoshimura, N. Leakage current characterization for estimating the conditions of ceramic and polymeric insulating surfaces. *IEEE Trans. Dielectr. Electr. Insul.* **2004**, *11*, 681–690. [CrossRef]

72. Du, B.; Liu, Y.; Liu, H.; Yang, Y. Recurrent plot analysis of leakage current for monitoring outdoor insulator performance. *IEEE Trans. Dielectr. Electr. Insul.* **2009**, *16*, 139–146. [CrossRef]

73. Hui, A.; Zheng, J.; Lin, H.; He, B. Wavelet-fractal characteristics of leakage current on HV insulators. In Proceedings of the 2008 Third International Conference on Electric Utility Deregulation and Restructuring and Power Technologies, Nanjing, China, 6–9 April 2008; pp. 732–736.

74. Natarajan, A.; Narayanan, S. S-transform based time-frequency analysis of leakage current signals of transmission line insulators under polluted conditions. *J. Electr. Eng. Technol.* **2015**, *10*, 616–624. [CrossRef]

75. Kannan, K.; Shivakumar, R.; Chandrasekar, S. A Random Forest Model Based Pollution Severity Classification Scheme of High Voltage Transmission Line Insulators. *J. Electr. Eng. Technol.* **2016**, *11*, 951–960. [CrossRef]

76. Khaled, A.; El-Hag, A.; Assaleh, K. Equivalent salt deposit density prediction of outdoor polymer insulators during salt fog test. In Proceedings of the 2016 IEEE Conference on Electrical Insulation and Dielectric Phenomena (CEIDP), Toronto, ON, Canada, 16–19 October 2016; pp. 786–789.

77. Xia, Y.; Song, X.; Jia, Z.; Wang, X.; Li, Y. Applying S-transform and SVM to evaluate insulator's pollution condition based on leakage current. In Proceedings of the 2018 12th International conference on the properties and applications of dielectric materials (ICPADM), Xi'an, China, 20–24 May 2018; pp. 742–747.

78. Deb, S.; Choudhury, N.R.; Ghosh, R.; Chatterjee, B.; Dalai, S. Short time modified Hilbert transform-aided sparse representation for sensing of overhead line insulator contamination. *IEEE Sens. J.* **2018**, *18*, 8125–8132. [CrossRef]

79. Deb, S.; Das, S.; Pradhan, A.K.; Banik, A.; Chatterjee, B.; Dalai, S. Estimation of contamination level of overhead insulators based on surface leakage current employing detrended fluctuation analysis. *IEEE Trans. Ind. Electron.* **2019**, *67*, 5729–5736. [CrossRef]

80. Sit, K.; Chakraborty, A.; Dalai, S.; Chatterjee, B.; Pradhan, A.K. Mathematical Morphology aided Random Forest Classifier based High Voltage Porcelain Insulator Contamination level Classification. In Proceedings of the 2020 IEEE Region 10 Symposium (TENSYMP), Dhaka, Bangladesh, 5–7 June 2020; pp. 98–101.

81. Mussina, D.; Irmanova, A.; Jamwal, P.K.; Bagheri, M. Multi-Modal Data Fusion Using Deep Neural Network for Condition Monitoring of High Voltage Insulator. *IEEE Access* **2020**, *8*, 184486–184496. [CrossRef]

82. Castillo-Sierra, R.; Oviedo-Trespalacios, O.; Candelo-Becerra, J.E.; Soto, J.D.; Calle, M. A novel method for prediction of washing cycles of electrical insulators in high pollution environments. *Int. J. Electr. Power Energy Syst.* **2021**, *130*, 107026. [CrossRef]

83. Ma, D.; Jin, L.; He, J.; Gao, K. Classification of partial discharge severities of ceramic insulators based on texture analysis of UV pulses. *High Volt.* **2021**, *6*, 986–996. [CrossRef]

84. Sit, K.; Das, A.K.; Mukherjee, D.; Haque, N.; Deb, S.; Pradhan, A.K.; Dalai, S.; Chatterjee, B. Condition Monitoring of Overhead Polymeric Insulators Employing Hyperbolic Window Stockwell Transform of Surface Leakage Current Signals. *IEEE Sens. J.* **2021**, *21*, 10957–10964. [CrossRef]

85. Sun, J.; Zhang, H.; Li, Q.; Liu, H.; Lu, X.; Hou, K. Contamination degree prediction of insulator surface based on exploratory factor analysis-least square support vector machine combined model. *High Volt.* **2020**, *6*, 264–277. [CrossRef]

86. Palangar, M.F.; Mohseni, S.; Mirzaie, M.; Mahmoudi, A. Designing an Automatic Detector Device to Diagnose Insulator State on Overhead Distribution lines. *IEEE Trans. Ind. Inf.* **2021**, *18*, 1072–1082. [CrossRef]

87. Hui, L.; Qinghe, S.; Jun, Y.; Hailei, M. Detection and processing for±660 composite insulator abnormal discharge. In Proceedings of the 2014 International Conference on Power System Technology, Chengdu, China, 20–22 October 2014; pp. 1404–1409.

88. Tian, Z.; Jin, L.; Peng, C.; Duan, W.; Gao, K. Discrimination of transmission line insulator contamination grades using visible light images. In Proceedings of the 2016 IEEE 16th International Conference on Environment and Electrical Engineering (EEEIC), Florence, Italy, 7–10 June 2016; pp. 1–5.

89. Jarrar, I.; Assaleh, K.; El-Hag, A.H. Using a pattern recognition-based technique to assess the hydrophobicity class of silicone rubber materials. *IEEE Trans. Dielectr. Electr. Insul.* **2014**, *21*, 2611–2618. [CrossRef]

90. Yao, X.; Zhang, Y.; Gao, Y.; Pan, Y.; Liu, L. Research on technology of contact insulator pollution classification and pollution level division based on machine vision. In Proceedings of the 2017 IEEE 3rd Information Technology and Mechatronics Engineering Conference (ITOEC), Chongqing, China, 3–5 October 2017; pp. 1264–1268.

91. Patel, I.; Maarouf, I.; Soltan, S.; Saad, A.; Al-Taher, A.; El-Hag, A.; Assaleh, K. Image processing based estimation of ceramic insulator pollution levels. In Proceedings of the 2018 5th International Conference on Electric Power and Energy Conversion Systems (EPECS), Kitakyushu, Japan, 23–25 April 2018; pp. 1–4.

92. Chen, T.; Li, F.; Wei, Z.; Li, Z. Contamination Identification and Classification on Composite Insulator by Visible Light Images. In Proceedings of the 2020 IEEE International Conference on High Voltage Engineering and Application (ICHVE), Beijing, China, 6–10 September 2020; pp. 1–4.

93. Yan, S.J.; Duan, W.S.; Shan, H.T.; Tong, M.S. Insulator Contamination Measurement Based on Infrared Thermal and Visible Image Information Fusion. In Proceedings of the 2019 PhotonIcs & Electromagnetics Research Symposium-Spring (PIERS-Spring), Rome, Italy, 17–20 June 2019; pp. 1006–1011.

94. He, H.; Luo, D.; Lee, W.-J.; Zhang, Z.; Cao, Y.; Lu, T. A contactless insulator contamination levels detecting method based on infrared images features and RBFNN. *IEEE Trans. Ind. Appl.* **2018**, *55*, 2455–2463. [CrossRef]

95. Liu, L.; Mei, H.; Guo, C.; Tu, Y.; Wang, L. Pixel-Level Classification of Pollution Severity on Insulators Using Photothermal Radiometry and Multiclass Semisupervised Support Vector Machine. *IEEE Trans. Ind. Inf.* **2020**, *17*, 441–449. [CrossRef]

96. Suhaimi, S.M.I.; Bashir, N.; Muhamad, N.A.; Rahim, N.N.A.; Ahmad, N.A.; Rahman, M.N.A. Surface discharge analysis of high voltage glass insulators using ultraviolet pulse voltage. *Energies* **2019**, *12*, 204. [CrossRef]

97. Zhang, D.; Chen, S. Intelligent Recognition of Insulator Contamination Grade Based on the Deep Learning of Ultraviolet Discharge Image Information. *Energies* **2020**, *13*, 5221. [CrossRef]

98. Lu, F.; Wang, S.; Li, H. Insulator pollution grade evaluation based on ultraviolet imaging and fuzzy logic inference. In Proceedings of the 2010 Asia-Pacific Power and Energy Engineering Conference, Chengdu, China, 28–31 March 2010; pp. 1–4.

99. Yin, C.; Xiao, Z.; Guo, Y.; Shi, C.; Zhang, X.; Wu, G. Method for detecting the pollution degree of naturally contaminated insulator based on hyperspectral characteristics. *High Volt.* **2021**, *6*, 1031–1039. [CrossRef]

100. Tian, Z.; Jin, L.; Zhang, Y.; Ai, J.; Peng, C.; Duan, W. Discrimination of insulator contamination grades using information fusion of multi-light images. In Proceedings of the 2015 IEEE 11th International Conference on the Properties and Applications of Dielectric Materials (ICPADM), Sydney, Australia, 19–22 July 2015; pp. 967–970.

101. Qiu, Y.; Wu, G.; Xiao, Z.; Guo, Y.; Zhang, X.; Liu, K. An extreme-learning-machine-based hyperspectral detection method of insulator pollution degree. *IEEE Access* **2019**, *7*, 121156–121164. [CrossRef]

102. Xia, C.; Ren, M.; Wang, B.; Dong, M.; Song, B.; Hu, Y.; Pischler, O. Acquisition and analysis of hyperspectral data for surface contamination level of insulating materials. *Measurement* **2021**, *173*, 108560. [CrossRef]

103. Liu, Y.; Pei, S.; Fu, W.; Zhang, K.; Ji, X.; Yin, Z. The discrimination method as applied to a deteriorated porcelain insulator used in transmission lines on the basis of a convolution neural network. *IEEE Trans. Dielectr. Electr. Insul.* **2017**, *24*, 3559–3566. [CrossRef]

104. Tao, G.; Lianggang, X.; Hongyun, S.; Fengxiang, C.; Shichun, W.; Xiaowei, L. Research on Zero-Sequence Insulator Detection Technology Based on Deep Learning. *J. Physics Conf. Ser.* **2019**, *1325*, 012011. [CrossRef]

105. Waleed, D.; Mukhopadhyay, S.; Tariq, U.; El-Hag, A.H. Drone-Based Ceramic Insulators Condition Monitoring. *IEEE Trans. Instrum. Meas.* **2021**, *70*, 6007312. [CrossRef]

106. Stefenon, S.F.; Ribeiro, M.H.D.M.; Nied, A.; Mariani, V.C.; Coelho, L.D.S.; Leithardt, V.R.Q.; Silva, L.A.; Seman, L.O. Hybrid Wavelet Stacking Ensemble Model for Insulators Contamination Forecasting. *IEEE Access* **2021**, *9*, 66387–66397. [CrossRef]

107. Liu, Y.; Lai, T.; Liu, J.; Li, Y.; Pei, S.; Yang, J. Insulator Contamination Diagnosis Method Based on Deep Learning Convolutional Neural Network. In Proceedings of the 2021 3rd Asia Energy and Electrical Engineering Symposium (AEEES), Chengdu, China, 26–29 March 2021; pp. 184–188.

108. Zhao, Y.; Yan, J.; Wang, Y.; Jing, Q.; Liu, T. Porcelain Insulator Crack Location and Surface States Pattern Recognition Based on Hyperspectral Technology. *Entropy* **2021**, *23*, 486. [CrossRef]

109. He, Y.; Li, M.; Meng, Z.; Chen, S.; Huang, S.; Hu, Y.; Zou, X. An overview of acoustic emission inspection and monitoring technology in the key components of renewable energy systems. *Mech. Syst. Sig. Process.* **2021**, *148*, 107146. [CrossRef]

110. Pei, C.; Shu, N.; Li, L.; Li, Z.; Peng, H. On-line monitoring of insulator contamination causing flashover based on acoustic emission. In Proceedings of the 2008 Third International Conference on Electric Utility Deregulation and Restructuring and Power Technologies, Nanjing, China, 6–9 April 2008; pp. 1667–1671.

111. Li, H.; Wen, X.; Shu, N.; Pei, C. Application of Acoustic Emission Technology on Monitoring of Polluted Insulator Discharge. In Proceedings of the 2009 Asia-Pacific Power and Energy Engineering Conference, Wuhan, China, 28–30 March 2009; pp. 1–4.

112. Jiang, Y.; McMeekin, S.G.; Reid, A.J.; Nekahi, A.; Judd, M.D.; Wilson, A. Monitoring insulator contamination level under dry condition with a microwave reflectometer. In Proceedings of the 2015 IEEE 11th International Conference on the Properties and Applications of Dielectric Materials (ICPADM), Sydney, Australia, 19–22 July 2015; pp. 959–962.

113. Yi, M.C.; Fang, J.; Wang, Y.; Li, Z.N.; Gu, C.H.; Shu, N.Q.; Li, Z.P. A Method for Extracting Acoustic Emission Signal Frequency Characteristics of Polluted-Insulator Discharge. *Appl. Mech. Mater.* **2014**, *494–495*, 1513–1516. [CrossRef]

114. Al-geelani, N.A.; Piah, M.A.M.; Abdul-Malek, Z. Identification of acoustic signals of corona discharges under different contamination levels using wavelet transform. *Electr. Eng.* **2018**, *100*, 1059–1067. [CrossRef]

115. El-Hag, A.H. Promoting condition monitoring and diagnostics of electrical insulation in undergraduate capstone graduation projects. *IEEE Electr. Insul. Mag.* **2015**, *31*, 8–15. [CrossRef]

116. Qaddoumi, N.N.; El-Hag, A.H.; Saker, Y. Outdoor insulators testing using artificial neural network-based near-field microwave technique. *IEEE Trans. Instrum. Meas.* **2013**, *63*, 260–266. [CrossRef]

117. Stefenon, S.F.; Grebogi, R.B.; Freire, R.Z.; Nied, A.; Meyer, L.H. Optimized ensemble extreme learning machine for classification of electrical insulators conditions. *IEEE Trans. Ind. Electron.* **2019**, *67*, 5170–5178. [CrossRef]

118. Frizzo Stefenon, S.; Zanetti Freire, R.; dos Santos Coelho, L.; Meyer, L.H.; Bartnik Grebogi, R.; Gouvêa Buratto, W.; Nied, A. Electrical insulator fault forecasting based on a wavelet neuro-fuzzy system. *Energies* **2020**, *13*, 484. [CrossRef]

119. Su, H.; Jia, Z.; Guan, Z.; Li, L. Mechanism of contaminant accumulation and flashover of insulator in heavily polluted coastal area. *IEEE Trans. Dielectr. Electr. Insul.* **2010**, *17*, 1635–1641. [CrossRef]

120. Yang, S.; Jia, Z.; Ouyang, X.; Bai, H.; Zhang, X. Effects of algae contamination on composite insulator hydrophobic property. In Proceedings of the 2017 1st International Conference on Electrical Materials and Power Equipment (ICEMPE), Xi'an, China, 14–17 May 2017; pp. 667–670.

121. Yang, S.; Jia, Z.; Ouyang, X. Effects of algae contamination on the hydrophobicity of high-voltage composite insulators. *High Volt.* **2019**, *4*, 234–240. [CrossRef]

122. Dave, V.; Gupta, H.; Chandra, R. Nanostructured hydrophobic DC sputtered inorganic oxide coating for outdoor glass insulators. *Appl. Surf. Sci.* **2014**, *295*, 231–239. [CrossRef]

123. Zeng, X.; Wang, X.; Cheng, L.; Zhang, S.; Liao, R. A Research on the Super-hydrophobic Surface Constructing Method for the Out-door Insulator Based on the Recycling of Composite. In Proceedings of the 2018 IEEE International Conference on High Voltage Engineering and Application (ICHVE), Athens, Greece, 10–13 September 2018; pp. 1–4.

124. Bala, P.; Bose, R.; Chatterjee, S. Electric stress analysis of a 11kV RTV silicone rubber coated porcelain insulator. In Proceedings of the 2016 Biennial International Conference on Power and Energy Systems: Towards Sustainable Energy (PESTSE), Bengaluru, India, 21–23 January 2016; pp. 1–6.

125. Yang, Z.; Jia, Z.; Chen, C.; Zhang, X.; Liu, L.; Zhu, R.; Xie, Q. Hydrophobicity distribution analysis of DC composite insulators. In Proceedings of the 2014 IEEE Electrical Insulation Conference (EIC), Philadelphia, PA, USA, 8–11 June 2014; pp. 465–468.

126. Chandrasekar, S.; Kalaivanan, C.; Montanari, G.C.; Cavallini, A. Partial discharge detection as a tool to infer pollution severity of polymeric insulators. *IEEE Trans. Dielectr. Electr. Insul.* **2010**, *17*, 181–188. [CrossRef]

127. Liu, Y.; Du, B. Energy eigenvector analysis of surface discharges for evaluating the performance of polymer insulator in presence of water droplets. *IEEE Trans. Dielectr. Electr. Insul.* **2014**, *21*, 2438–2447. [CrossRef]

128. Hussain, M.M.; Farokhi, S.; McMeekin, S.; Farzaneh, M. Prediction of surface degradation of composite insulators using PD measurement in cold fog. In Proceedings of the 2016 IEEE International Conference on Dielectrics (ICD), Montpellier, France, 3–7 July 2016; pp. 697–700.

129. Al Khafaf, N.; El-Hag, A. Bayesian regularization of neural network to predict leakage current in a salt fog environment. *IEEE Trans. Dielectr. Electr. Insul.* **2018**, *25*, 686–693. [CrossRef]

130. Jinlei, H.; Chao, S.; Zhenxing, K.; Xiaobo, Z.; Yunpeng, J. Insulator Contamination Prediction Model Based on BP Neural Network Optimized by Genetic Algorithm. In Proceedings of the 2018 International Conference on Power System Technology (POWERCON), Guangzhou, China, 6–8 November 2018; pp. 3166–3172.

131. Yan, S.; Gang, H.; Jiafu, Z. The Monitoring Interface of Insulator's State Based on the Leakage Characteristics. In Proceedings of the 2020 IEEE International Conference on High Voltage Engineering and Application (ICHVE), Beijing, China, 6–10 September 2020; pp. 1–4.

132. Liu, Y.; Yang, J.; Li, Y.; Pei, S.; Liu, J.; Lai, T. Research on Diagnosis Device of Insulator Pollution Degree Based on BP Neural Network. In Proceedings of the 2021 3rd Asia Energy and Electrical Engineering Symposium (AEEES), Chengdu, China, 26–29 March 2021; pp. 166–169.

133. Zhao, S.; Jiang, X.; Xie, Y. Evaluating the contamination level of polluted insulators based on the characteristics of leakage current. *Int. Trans. Electr. Energy Syst.* **2015**, *25*, 2109–2123. [CrossRef]

134. Mahdjoubi, A.; Zegnini, B.; Belkheiri, M.; Seghier, T. Fixed least squares support vector machines for flashover modelling of outdoor insulators. *Electr. Power Syst. Res.* **2019**, *173*, 29–37. [CrossRef]

135. Zhou, H.; Chen, Y. Prediction of Insulator Pollution Flashover Voltage Based on Data Mining Technology. *IOP Conf. Series Earth Environ. Sci.* **2021**, *692*, 022070. [CrossRef]

136. Chaou, A.K.; Mekhaldi, A.; Teguar, M. Recurrence quantification analysis as a novel LC feature extraction technique for the classification of pollution severity on HV insulator model. *IEEE Trans. Dielectr. Electr. Insul.* **2015**, *22*, 3376–3384. [CrossRef]

137. Corso, M.P.; Perez, F.L.; Stefenon, S.F.; Yow, K.-C.; García Ovejero, R.; Leithardt, V.R.Q. Classification of Contaminated Insulators Using k-Nearest Neighbors Based on Computer Vision. *Computers* **2021**, *10*, 112. [CrossRef]

138. Feng, H.; Xuran, H.; Bin, L.; Haipeng, W.; Decai, Z. Infrared Image Recognition Technology Based on Visual Processing and Deep Learning. In Proceedings of the 2020 Chinese Automation Congress (CAC), Shanghai, China, 6–8 November 2020; pp. 641–645.

139. Vigneshwaran, B.; Maheswari, R.; Kalaivani, L.; Shanmuganathan, V.; Rho, S.; Kadry, S.; Lee, M.Y. Recognition of pollution layer location in 11 kV polymer insulators used in smart power grid using dual-input VGG Convolutional Neural Network. *Energy Rep.* **2021**, *7*, 7878–7889. [CrossRef]

140. Wang, Y.-C.; Lin, Y.-T.; Chang, H.-C.; Kuo, C.-C. Contamination assessment of insulators using microsystem technology with fuzzy-based approach. *Microsyst. Technol.* **2019**, *27*, 1759–1772. [CrossRef]

141. Petri, L.d.P.S.; Moutinho, E.A.; Silva, R.P.; Capelini, R.M.; Salustiano, R.; Ferraz, G.M.F.; Neto, E.T.W.; Villibor, J.P.; Pinto, S.S. A Portable System for the Evaluation of the Degree of Pollution of Transmission Line Insulators. *Energies* **2020**, *13*, 6625. [CrossRef]

142. Lu, Y.-P.; Yu, M.; Lai, L.; Lin, X. A new fuzzy neural network based insulator contamination detection. In Proceedings of the 2006 International Conference on Machine Learning and Cybernetics, Dalian, China, 13–16 August 2006; pp. 4099–4104.

143. Salem, A.A.; Abd Rahman, R.; Kamarudin, M.; Othman, N.; Jamail, N.; Hamid, H.; Ishak, M. An alternative approaches to predict flashover voltage on polluted outdoor insulators using artificial intelligence techniques. *Bull. Electr. Eng. Inform.* **2020**, *9*, 533–541. [CrossRef]

144. Singh, P.; Dutta, S.; Baral, A.; Chakravorti, S. Contamination Level Assessment in Porcelain Disc Insulator using Detrended Fluctuation Analysis. In Proceedings of the 2019 IEEE 4th International Conference on Condition Assessment Techniques in Electrical Systems (CATCON), Chennai, India, 21–23 November 2019; pp. 1–5.

145. Dey, J.; Dutta, S.; Baral, A.; Chakravorti, S. Leakage Current Monitoring of Suspension Insulator for Effective Determination of ESDD. In Proceedings of the 2019 8th International Conference on Power Systems (ICPS), Jaipur, India, 20–22 December 2019; pp. 1–6.

146. Liao, Y.; Li, Y.; Zhang, F.; Zhang, X.; Wang, T.; Guo, Y.; Xiao, Z.; Wang, Y. Study on evaluation method of insulator surface contamination level based on LIBS technology and PCA algorithm. In Proceedings of the 2019 2nd International Conference on Electrical Materials and Power Equipment (ICEMPE), Guangzhou, China, 7–10 April 2019; pp. 512–517.

147. Ahmad, J.; Tahir, A.; Stewart, B.G.; Nekahi, A. Forecasting Flashover Parameters of Polymeric Insulators under Contaminated Conditions Using the Machine Learning Technique. *Energies* **2020**, *13*, 3889.
148. Palangar, M.; Mirzaie, M. Predicting Critical Conditions in Polluted Insulators Using Phase Angle Index of Leakage Current. In Proceedings of the 2020 IEEE International Conference on High Voltage Engineering and Application (ICHVE), Beijing, China, 6–10 September 2020; pp. 1–4.
149. Salem, A.A.; Abd-Rahman, R.; Al-Gailani, S.A.; Salam, Z.; Kamarudin, M.S.; Zainuddin, H.; Yousof, M.F.M. Risk assessment of polluted glass insulator using leakage current index under different operating conditions. *IEEE Access* **2020**, *8*, 175827–175839. [CrossRef]
150. Wahyudi, M.; Setiawan, N.A.; Pambudi, K.; Saputra, D. Severity Level of An Insulator in Polluted and Dry Conditions Based on Ultraviolet Emission. In Proceedings of the 2020 2nd International Conference on Smart Power & Internet Energy Systems (SPIES), Bangkok, Thailand, 2–4 June 2020; pp. 457–462.
151. Banik, A.; Nielsen, S.; Nourbakhsh, G. A crest factor-based technique for the analysis of polluted insulator leakage current under harmonically distorted supply voltage. *Electr. Eng.* **2021**, *103*, 1823–1836. [CrossRef]